# Laser Light Scattering Studies of Some Special Polymers in Solution

By

Kwan Chi Man Simon (關志文)

A thesis submitted to the Chemistry Division,
Graduate School, the Chinese University of Hong Kong
in partial fulfilment of the requirements
for the degree of
Master of Philosophy.

(1997)

Thesis Committee:

Dr. Steve C.F. Au-Yeung

Dr. Raymund W. M. Kwok

Dr. Chi Wu

Prof. Hanjie Hu (External Examiner)

## Abstract

Laser light scattering (LLS) was used to investigate the following special polymers: (1) two sets of high performance soluble polyimides; and (2) a series of optically active conjugated polyarylenes and poly(aryleneethnylene)s.

Two sets of broadly distributed soluble high performance polyimides synthesized from 2,2'-bis(3,4'-dicarboxyphenyl)hexafluoro-propane dianhydride (6FDA) and 2,2'-(trifluoromethyl)-4,4'-diaminobiphenyl diamine (PFMB), and from 2,2'-bis(trifluoromethyl)-4,4',5,5'-biphenyl-tetracarboxylic dianhydride (HFBPDA) and 2,2'-(trifluoromethyl)-4,4'-diaminobiphenyl diamine (PFMB) were investigated by static and dynamic LLS in THF at 30°C. Weight-average molar mass $M_w$, second virial coefficient $A_2$ and root mean square z-average radius of gyration $\langle R_g^2 \rangle_z^{1/2}$ (or simply $\langle R_g \rangle$) were obtained by static LLS. The z-average translational diffusion coefficient $\langle D \rangle$ or average hydrodynamic radius $\langle R_h \rangle$ was obtained by measuring the intensity-intensity time correlation function $G^{(2)}(t)$ in dynamic LLS. A method of combining static and dynamic light scattering enables us to obtain the calibrations of $D\ (cm^2/s) = 2.41 \times 10^{-4} M^{-0.564}$ and $D\ (cm^2/s) = 6.16 \times 10^{-4} M^{-0.656}$ respectively for 6FDA-PFMB and HFBPDA-PFMB, where D and M are the translational diffusion coefficient and the molar mass for monodisperse species, respectively. With these calibrations, we can convert each translational diffusion coefficient distribution G(D) into a corresponding molar mass distribution $f_w(M)$. The persistence length were found to be 3.3 and 4.5 nm respectively for 6FDA-PFMB and HFBPDA-PFMB on the basis of the Kratky-Porod wormlike chain model. In addition, $\langle R_g \rangle / \langle R_h \rangle \sim$ (1.7~1.9) shows that they are in coil conformation. We concluded that, although there

exist rigid segments in their backbone chains, these polymers behave as an expanded random coil in solution.

A series of optically active conjugated polyarylenes and poly(aryleneethnylene)s were characterized by a combination of laser light scattering and off-line gel permeation chromatography (GPC) using only one broadly distributed sample. This method enables us to obtain not only $M_w$, $A_2$, $\langle R_g \rangle$, $\langle D \rangle$ and $\langle R_h \rangle$, but also two calibrations: $V = A + B\log(M)$ and $D = k_D M^{-\alpha_D}$ for each of the polymers, where V is the elution volume, and A, B, $k_D$and $\alpha_D$ are calibration constants. With these calibrations, we were able to transform C(V) from GPC or G(D) from dynamic LLS to $f_w(M)$, where C(V) is the distribution of the elution volume in GPC. Comparing $M_w$ measured from LLS with that from GPC shows that the calibration of the GPC column by polystyrene standard was improper because the polystyrene standard and the polymers studied have quite different chain conformations in solution. The fact that $\alpha_D = 1$ indicates that all the conjugated polymers studied have a rigid-rod chain conformation in THF at 25°C.

# 摘要

本文采用激光光散射(LLS)方法研究了以下特殊高分子: (1) 两系列高性能可溶性聚　亚胺, 它们分别由单体2,2'-双(3,4'-二羧基苯基)六氟丙烷二酐(6FDA)与 2,2'-(三氟甲基)-4,4'-二氨基联苯二氨(PFMB), 以及 2,2'-双(三氟甲基)-4,4',5,5'-联苯四羧基二酐(HFBPDA)与 2,2'-(三氟甲基)-4,4'-二氨基联苯二氨(PFMB)缩聚合成. 在 30°C 的 THF 溶液中用静态光散射方法测定了上述聚合物的重均分子量 $M_w$, 第二维利系数 $A_2$ 和均方旋转半径$\langle R_g^2\rangle_z^{1/2}$. 并以动态光散射的光强-时间相关函数 $G^{(2)}(t)$测得其平动扩散系数$\langle D\rangle$和流体力学半径$\langle R_h\rangle$. 结合静态和动态光散射的结果, 我们得到了 6FDA-PFMB 和 HFBPDA-PFMB 两类聚合物的 D ~ M 关系分别为 $D(cm^2/s) = 2.41\times10^{-4}M^{-0.564}$ 和 $D(cm^2/s) = 6.16\times10^{-4}M^{-0.656}$. 由上述关系式, 我们进一步将平动扩散系数的分布 G(D)转换得到对应的摩尔质量分布 $f_w(M)$. 根据 Kratky-Porod 蠕虫链模型计算得到 6FDA-PFMB 和 HFBPDA-PFMB 的链持久长度分别为 3.3 和 4.5nm. 此外, $\langle R_g\rangle/\langle R_h\rangle$的比值(1.7 ~ 1.9)表明这两类聚合物在溶液中的构象为伸展的无规线团.

(2) 一系列具有光学活性共轭聚芳烃和聚芳烯烃. 通过将 LLS 与凝胶渗透色谱(GPC)联用, 我们不但得到聚合物的 $M_w$, $A_2$, $\langle R_g^2\rangle_z^{1/2}$, $\langle D\rangle$和$\langle R_h\rangle$, 而且还得到淋洗体积(V)与分子量 M 的校正关系 V = A + Blog(M), 以及扩散系数与分子量的关系 $D = k_D M^{-\alpha D}$, 其中 A, B, $k_D$ 及$\alpha_D$ 是关系常数. 采用这些校正关系, 我们将 GPC 的 C(V)和 LLS 的 G(D)分布转化为 $f_w(M)$分布. 常数$\alpha_D$=1 表明这些共轭高分子在 25°C 的 THF 溶液中为刚性棒状构象, 不同于聚苯乙烯的无规线团. 因此用聚苯乙烯标样测得的聚芳烃和聚乙烯芳烃分子量与实际值有一定的差别.

**Acknowledgments**

I would like to express my sincere thanks to my supervisor Dr. Chi WU for his invaluable advice, guidance and encouragement during the course of research and the preparation of this thesis.

Thanks are also given to the graduate students and visiting scholars Chan Kam-kwong, Zhou Shui-qin, Zhang Yu-bao, Mahammad Siddiq, Gao Jun, Qiu Xing-ping, Wang Xiao-hua, Gan Zhi-hua, and Jiang so-hung in our laboratory for their assistance and helpful discussions.

I specially thank to Prof. Stephen Z.D. Cheng in the University of Akron and Prof. Pu Lin in the North Dakota State University for providing samples for me to investigate.

I am also indebted to my family and Kwan-yee for their deep love and strong moral support during my two years study.

This financial support by the RGC (the Research Grants Council of the Hong Kong Government) Earmarked Grant is gratefully acknowledged.

June, 1997

Kwan Chi Man Simon

Department of Chemistry

The Chinese University of Hong Kong

**Contents**

## Abbreviations

| | |
|---|---|
| 6FDA-PFMB | Polyimide synthesized from 2,2'-bis(3,4-dicarboxyphenyl)-hexafluoro-propane dianhydride (6FDA) and 2,2'-(trifluoromethyl)-4,4'diaminobiphenyl diamine (PFMB). |
| A | The measured baseline. (Ch.2.2 and A.2) |
| A | Free energy. (Ch.A.1) |
| A | Calibration constant between V and M. (Ch.2.6 and 5) |
| $A_2$ | Second virial coefficient. |
| $A_j(t)$ | Amplitude of scattered light from molecule j. |
| b | Independent varible. |
| $b_o$ | value of b when the free energy A is at a minimun. |
| B | Calibration constants between V and M. |
| $\overline{(\delta b)^2}$ | Mean square of the fluctuation of the indepentent varible. |
| C | Concentration of polymer solutions. |
| C(V) | Distribution of elution volume |
| $\delta C$ | Fluctuation of concentration. |
| $\overline{(\delta C)^2}$ | Mean square of the fluctuation of concentration. |
| $C_A(t)$ | Amplitude correlation function. |
| $C_\psi(t)$ | Phase correlation function. |
| $C_D$ | Empirical positive constant. |
| $C_\infty$ | Characteristic ration. |
| D | Translational diffusion coefficient. |
| dn/dc | The specific refractive index increment. |

| | |
|---|---|
| $\langle D \rangle$ | z-average translational diffusion coefficient. |
| $\langle \lvert E_s \rvert \rangle^2$ | Time average of the electric field. |
| $\mathbf{E}_s$, $E_s(t)$, $E(t)$ | Scattered electric field. |
| $f(M)$ | Number distribution of molar mass. |
| $f_w(M)$ | Weight distribution of molar mass. |
| $f$ | A dimensionless number depending the angular dependence of $\langle D \rangle$. (Ch.2.2 and A.2.2) |
| $f$ | Molecular friction factor. (Ch.A.2) |
| GPC | Gel permeation chromatography |
| $G^{(1)}(t)$ | First-order electric field time correlation function. |
| $G^{(1)}(0)$ | First-order electric field time correlation function with zero delay time (average intensity). |
| $g^{(1)}(t)$ | Normalized first-order electric field time correlation function. |
| $G^{(2)}(t)$ | Intensity-intensity time correlation function. |
| $G(D)$ | Translational diffusion coefficient distribution. |
| $G(\Gamma)$ | Normalized linewidth distribution. |
| $G_s(\mathbf{r},t)$ | Intermediate structure factor. |
| HFBPDA-PFMB | Polyimide synthesized from 2,2'-bis(trifluoro-methyl)-4,4',5,5'-biphenyl-tetracarboxylic dianhydride (HFBPDA) and 2,2'-(trifluoromethyl)-4,4'-diaminobiphenyl diamine (PFMB). |
| $\langle h^2 \rangle$ | Mean square end-to-end distance. |
| $\langle h^2 \rangle_o$ | Mean square end-to-end distance at theta condition. |

| | |
|---|---|
| $\langle h^2 \rangle_f$ | Mean square end-to-end distance of a freely rotating chain. |
| $I_s$ | Scattered intensity. |
| $I_o$ | Intensity of incident light. |
| $\langle I_s \rangle$ or $\langle I \rangle$ | Time average scattered intensity. |
| $\langle I \rangle_{solution}$ | Time average scattered intensity of solution. |
| $\langle I \rangle_{solvent}$ | Time average scattered intensity of solvent. |
| $k_m$ | $m^{th}$ cumulant of $g^{(1)}(t)$. |
| $\mathbf{k}$ | $\mathbf{k}_s - \mathbf{k}_p$. |
| $\mathbf{k}_p$ | Unit vector along transmiting direction. |
| $\mathbf{k}_s$ | Unit vector along scattering direction. |
| $k_d$ | The diffusion second virial coefficient. |
| k | The Boltzmann constant. |
| $k_D$ | Calibration constant between D and M |
| K | Optical constant |
| L | Contour length. |
| $\Delta L$ | Lenght of segment |
| LLS | Laser light scattering. |
| $l_u$ | Projection length of monomer unit. |
| M | Molar mass for monodisperse. |
| $M_w$ | Weight-average molar mass. |
| $(M_w)_{calcd}$ | The calculated weight-average molar mass. |
| $M_o$ | Monomer mass. |

| | |
|---|---|
| MEK | Methy ethyl ketone. |
| n | Number of scattering points in a particle. (Ch.A.1.2) |
| n | Slovent refractive index. (Ch.2.1) |
| n | Degree of polymerization (Ch.4.3) |
| $\langle n \rangle$ | Average number of photons counted in time $\Delta t$. |
| $\Delta n$ | Refractive index increment. |
| N | Number of carbon-carbon bonds (Ch.4.3) |
| N | Number of main chain bonds (Ch.2.2.1 and 2.4.2) |
| N | Number of molecules in unit volume. (Ch.A.1.3.1) |
| N | Number of correlation channels (Ch.A.2.1) |
| $N_A$ | Avogadro's number. |
| p | Channel number |
| $P_1$ | Proportional constant. |
| $P(\theta)$ | Particle scattering factor. |
| r | Distance from the scattering particle to the detector. |
| $\mathbf{r}_{ij}$ | Position vector from point i to point j. |
| $R_g$ | Radius of gyration. |
| $\langle R_g^2 \rangle_z$ or $\langle R_g \rangle$ | Root mean square *z*-average radius of gyration. |
| $\langle R_g^2 \rangle_{oz}$ | Root mean square *z*-average radius of gyration at theta condition. |
| $\langle R_h \rangle$ | z-average hydrodynamic radius. |
| $R_o$ | The Rayleigh ratio at zero angle. |

| | |
|---|---|
| $R_{vv}$ | The Rayleigh ratio with both vertically polarized incident light and scattered light. |
| $\Delta R_{vv}$ | The excess Rayleigh ratio. |
| q | Scattering vector. |
| $q$ | Persistence length. |
| S(ω) | Scattered optical spectrum |
| $t$ | time. |
| t | delay time. |
| Δt | Channel width. |
| T | Absolute temperature. |
| THF | Tetrahydrofuran. |
| u | Polydispersity parameter |
| V | Volume of a subregion. |
| $V_e$ | Elution volume of intermediate pariles. |
| $V_o$ | Volume of the solvent exterior to the gel partiles. |
| $V_i$ | Internal volume of the pores. |
| Γ | Linewidth. |
| $\omega_o$ | Angular frequency of electric field. |
| μ | Chemical potential. |
| ϕ | volume fraction. (Ch.A.1.4) |
| ϕ | Rotation angle. (Ch.2.4.1) |
| ε | Dielectric constant. |

| | |
|---|---|
| $\overline{(\delta\varepsilon)^2}$ | Mean square of the fluctuation of dielectric constant. |
| $\rho$ | Density. |
| $\overline{(\delta\rho)^2}$ | Mean square of the fluctuation of density. |
| $\alpha$ | Polarizability of an isotropic particle. |
| $\alpha_D$ | Calibration constant between D and M |
| $\alpha_o$ | Polarizability of a scattering particle. |
| $\varphi$ | Phase difference of scattered light wave. |
| $\Delta_{ij}$ | Path difference of light scattered by two scattering points. |
| $\lambda_o$ | Wavelength of light in vacuum. |
| $\beta$ | The parameter depending on the coherence of the detection. (Ch.2.2) |
| $\beta$ | Isothermal compressibility. (Ch.A.1.3.1) |
| $\beta$ | Variable governing the average of molar mass. (Ch.2.3) |
| $\eta$ | Solvent viscosity. |
| $\psi_s$ or $\psi_s(t)$ | Phase of scattered field. |
| $\psi$ | Supplementary angle. |
| $\sigma$ | Fraction of the internal volume accessible to the solute. (Ch.2.3) |
| $\sigma$ | Conformation factor. (Ch.2.4.1) |
| $\theta$ | Scattering angle. |
| $\theta_1$ | 180° minus the fixed bond angle. |
| $\tau$ | Delay time |

## List of Figures

## List of Tables

# Chapter 1

## Introduction

Polyimides have been used in the electronic and aerospace industry due to their excellent thermal, chemical, electrical and mechanical properties. Recently, it has been found that the cost and the performance of liquid crystal displays can be greatly reduced and improved by introducing a thin film of polyimide in the display. Therefore, the molecular parameters, such as molar mass, size and polydispersity are very important to the development of polyimides. However, polyimides normally are not soluble in common organic solvent because they are usually very rigid. In the past, the molecular parameters of insoluble polyimides had to be estimated from their precursors. The estimation has some problems, such as the polyelectrolytes effect in the precursor solution and the structure discrepancy between the precursor and final polymer. Recently, direct light scattering investigations can be achieved because soluble high performance polyimides have been developed by introducing some side groups, such as $-CH_3$ and $-CF_3$, in the polymer chain to twist the aromatic imide rings and the phenyl groups, and some joints, such as -O- and $-CH_2-$, to separate the aromatic imide rings and the phenyl rings.

Chiral conjugated polymers are a class of potentially useful materials. There are two kinds of conjugated polymers: one has its chirality derived from the side-chain chiral substituents and the other one consists of inherently chiral configuration in the main chain. The latter may be applied to the area of asymmetric electrosynthesis, polarized photo- and electroluminescence, enantioselective sensing and asymmetric

catalysis. The optimization of the synthesis and development of various applications of the these polymers requires the characterization of their molecular parameters, such as molar mass distribution and chain flexibility. A combination of off-line laser light scattering and gel permeation chromatography is very suitable for characterizing these polymers because it requires only one boardly distributed sample where well-fractionated samples of these polymers are not easily obtained.

In the last two decades, light scattering has been developed into a very powerful tool to investigate the molecular parameters of polymers in solution, such as molar mass, interaction parameter and the size. It has become a common routine method in academic research and industrial development to characterize polymers and colloids. Owing to the development of lasers and advance electronic devices, dynamic light scattering has been well developed to probe the Brownian and internal motions of polymers in solution. Nowadays, a combination of static and dynamic light scattering can lead not only the weight-average molar mass $M_w$, the second virial coefficient $A_2$, the root mean square average radius of gyration $\langle R_g \rangle$, z-average translational diffusion coefficient $\langle D \rangle$ and average hydrodynamic radius $\langle R_h \rangle$, but also a calibration between D and M, i.e., $D = k_D M^{-\alpha_D}$, where D and M are for monodisperse. With this calibration, we can transform translational diffusion coefficient distribution G(D) into molar mass distribution $f_w(M)$. Furthermore, a combination of laser light scattering and gel permeation chromatography can simultaneously lead to two calibrations: $V = A + B\log(M)$ and $D = k_D M^{-\alpha_D}$ by using only one broadly distributed polymer sample, where V is the elution volume. With these calibrations, we again can obtain molar mass distribution $f_w(M)$ from C(V) in GPC or G(D) in dynamic LLS, where C(V) is distribution of elution volume.

This thesis has been arranged in the following order. Chapter 2 presents the basic theories of laser light scattering, gel permeation chromatography, polymer dynamics and data analysis.

Chapter 3 describes the instrumentation of laser light scattering, differential refractometer and gel permeation chromatography.

Chapter 4 summarizes the LLS studies of two sets of high performance soluble polyimides synthesized from 2,2'-bis(3,4'-dicarboxyphenyl)hexafluoropropane dianhydride (6FDA) and 2,2'-(trifluoromethyl)-4,4'-diaminobiphenyl diamine (PFMB) (6FDA-PFMB), and from 2,2'-bis(trifluoromethyl)-4,4',5,5'-biphenyl-tetracarboxylic dianhydride (HFBPDA) and 2,2'-(trifluoromethyl)-4,4'-diaminobiphenyl diamine (PFMB) (HFBPDA-PFMB) in THF at 30°C.

Chapter 5 discusses the characterization of various polyarylenes and poly(aryleneethnylene)s in THF at 25°C by using a method of combining off-line laser light scattering (LLS) and gel permeation chromatography (GPC).

Appendix gives the detailed theories of static and dynamic laser light scattering for reference.

# Chapter 2

## Theoretical background

In our daily life, the light scattering happens everywhere. For example, the blue color of sky is resulted from the fact that the blue light composed in the sun light is scattered much more by the particles in the atmosphere. Often, we see or measure a time-averaged scattered light intensity, i.e., *static light scattering*, which will be discussed in section 2.1. Static light scattering has been widely used to investigate the static properties of polymers in solution, such as molar mass, size and conformation. In reality, the frequency of the scattered light is slightly different from that of the incident light because of the Brownian motion of the polymer chains in solution. Therefore, the measurement of this small frequency shift enables us to probe the dynamics of polymer chains in solution such as the translational and rotational diffusion processes and the internal motions of a polymer chain. This method is often called quasi-elastic light scattering. In practice, instead of measuring the shift in frequency, we measure the intensity fluctuation in time domain. This is why it is also often called *dynamic light scattering*. The detailed theories of both static and dynamic laser light scattering is discussed in appendix.

*Gel permeation chromatography* (GPC) is a mostly used method for the determination of the molar mass distribution of polymers, which will be outlined in section 2.3. The bulk properties of polymers are related to the flexibility of polymer chains. In section 2.4, we will present some basic theories of the flexibility of polymer chains in solution. In section 2.5, we will detail a method of combining static and

dynamic light scattering results. Finally, a well-established procedure of combining laser light scattering and off-line gel permeation chromatography will be illustrated in section 2.6.

**2.1 Static laser light scattering (Static LLS).** In static LLS, the angular dependence of the excess absolute time-averaged scattered intensity, known as the excess Rayleigh ratio, $R_{vv}(q)$, was measured. For a dilute polymer solution measured at a low scattering angle, $R_{vv}(q)$ can be related to the weight-average molecular weight, $M_w$, the second virial coefficient, $A_2$, and root mean square z-average radius of gyration ,$\langle R_g^2 \rangle_z^{1/2}$ (or simply written as $\langle R_g \rangle$), as[1]

$$\frac{KC}{R_{vv}(q)} \approx \frac{1}{M_w}\left(1 + \frac{1}{3}\langle R_g^2 \rangle_z q^2\right) + 2A_2C \qquad (2.1.1)$$

where $K = 4\pi^2 n^2 (dn/dC)^2 / (N_A \lambda_0^4)$ and $q = (4\pi n/\lambda_0)\sin(\theta/2)$ with $N_A$, dn/dC, n and $\lambda_o$ being Avogadro number, the specific refractive index increment, the solvent refractive index and the wavelength of light in vacuo, respectively. Measuring $R_{vv}(q)$ at a set of C and q, we are able to determine $M_w$, $\langle R_g \rangle$, and $A_2$ from a Zimm plot which incorporates the extrapolation of $q \rightarrow 0$ and $C \rightarrow 0$ on a single grid.

**2.2 Dynamic laser light scattering (Dynamic LLS).** In dynamic LLS, a precise intensity-intensity time correlation function $G^{(2)}(t,q)$ in the self-beating mode was measured and $G^{(2)}(t,q)$ is related to the normalized first-order electric field time correlation function, $g^{(1)}(t,q)$ as [2]

$$G^{(2)}(t,q) = \langle I(t,q)I(0,q) \rangle = A[1 + \beta |g^{(1)}(t,q)|^2] \qquad (2.2.1)$$

where A is a measured base line; β, a parameter depending on the coherence of the detection; and t, the delay time. It is known that for a polydisperse sample $g^{(1)}(t,q)$ is related to the line-width distribution $G(\Gamma)$ by [2]

$$g^{(1)}(t,q) = < E(t,q)\, E^{*}(0,q) > = \int_0^{\infty} G(\Gamma)\, e^{-\Gamma t}\, d\Gamma \qquad (2.2.2)$$

The Laplace inversion program CONTIN was used normally to convert $G^{(2)}(t,q)$ to $G(\Gamma)$. The line width $\Gamma$ leads to the *z*-average translational diffusion coefficient D at $C \rightarrow 0$ by the Eq. (2.2.4)[3,4]

$$\Gamma / q^2 = D\,(1 + k_d C)\,(1 + f \langle R_g^2 \rangle_z q^2) \qquad (2.2.3)$$

where $k_d$ and $f$ are constant.

## 2.3 Gel Permeation Chromatography (GPC)[5]

GPC is a very convenient tools to measure molar mass M and molar mass distribution f(M) of polymers. GPC is very similar to high performance liquid chromatography. The main difference is only the material packed in the column. In GPC, the porous material is divided into small particles (10-1000 μm) and packed into a chromatographic column. The particles are porous and their size is the main characteristic of the column. Quite different materials are used. For aqueous solutions, the original gels were manufactured from cross-linked dextrin. For larger pores, low concentrated agarose gels are used.

The principle of GPC is simple. The solvent in the system is present in between the gel particles and inside the pores. When a solute with small molecules is added, it follows the solvent in both places. However, large solute molecules cannot penetrate into the pores and are forced to stay outside. Molecules of intermediate size can enter the larger pores but not the smaller ones. The situation is illustrated in Figure 2.3.1.

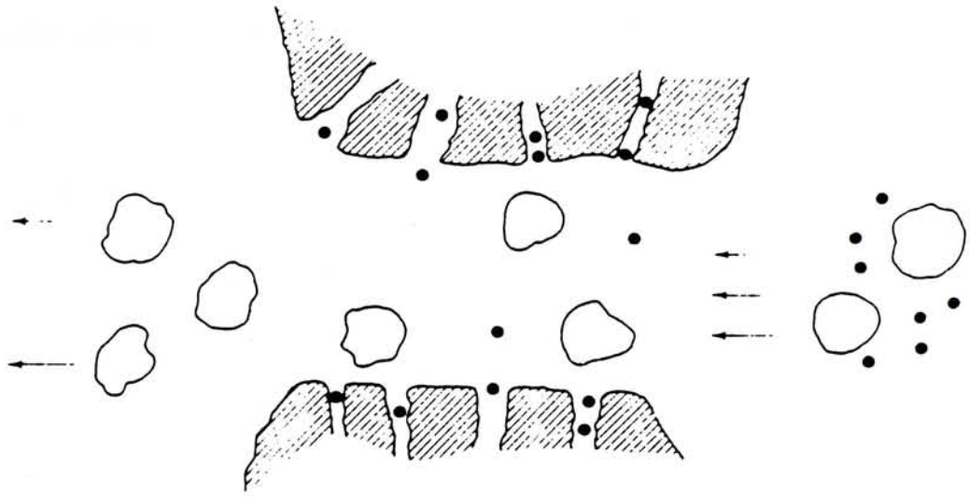

**Figure 2.3.1** A schematic description of the partitioning effect of pores on the separation of particles of different sizes in GPC

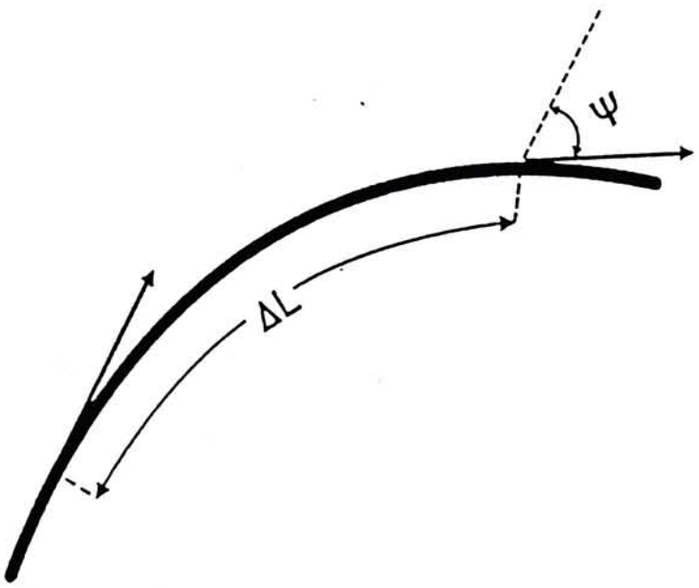


**Figure 2.4.1** A segment of a persistent chain

The distribution of the solute inside and outside of the gel is a typical partition phenomenon.

In the column, the volume of the solvent exterior to the gel particles is $V_o$; the internal volume of the pores is $V_i$. When a small amount of a polymer solution is applied on the column and is eluted in the usual way, the newly introduced solvent together with very small molecules is eluted after volume $V_t = V_o + V_i$ has passed through the column. Very large particles cannot penetrate into any pores; they travel faster than the solvent and elute with $V_o$ as their elution volume. The elution volume $V_e$ of intermediate particles is

$$V_e = V_o + \sigma V_i \qquad (2.3.1)$$

where $\sigma$ is the fraction of the internal volume accessible to the solute and depends on the nature of the gel and on the size of the solute molecules.

At the column outlet, a detector is equipped and usually registers some relevant properties of the elute. Ultraviolet spectrophotometers are very useful with UV-transparent solvents. Refractometry is used most often. All solutes exhibit an increment of refractive index that is proportional to the concentration of the solute. Nowadays, the combination of a refractometer and a low-angle laser light scattering spectrometer is a very powerful tools which is able to simultaneously measure the concentration and molecular weight as a function of the retention volume.

Using GPC to measure molar mass and molar mass distribution needs the calibration of the GPC column. It normally requires a set of narrowly distributed

polymer samples which are rather difficult, if not impossible, to obtain in practice. This is why polystyrene standards are often used if the polymer studied has a similar chain conformation in solution. Sometimes, the conformation of the polymer investigated is different from the calibration standard used, incorrect molar mass may be obtained. However, the most powerful characteristic of GPC is its ability to measure the molar mass distribution. The elution volume distribution is transformed into molar mass distribution by using the calibration curve. Once the distribution is obtained, different kind of averaging molar mass can be then calculated by

$$<M> = \int_o^\infty f_n(M)M^\beta \, dM \; / \; \int_o^\infty f_n(M)M^{\beta-1} \, dM \qquad (2.3.2)$$

where $\beta$ can be an integer number, such as $\beta = 1$ for the number-average molecular weight ($M_n$), $\beta = 2$ for the weight-average molecular weight ($M_w$) and $\beta = 3$ for intensity-average (or z-average) molecular weight ($M_z$).

## 2.4 Chain Flexibility[6]

In order to improve the performance of polymers and to understand the macroscopic properties of polymers, it is necessary to determine the flexibility of polymers in solution. Polymers exhibit conformations ranging from tight coils to highly extended structures such as rigid rods. The parameters and the methods used for evaluating the degree of chain flexibility are usually different for flexible and rigid chains. Therefore, we will discuss them in two sections.

**2.4.1 Flexible chains:** For flexible polymers the most common parameter used is Flory's[7-8] characteristic ratio $C_\infty$, which is defined as

$$C_\infty \equiv \lim_{N\to\infty} \frac{< h^2 >_o}{N\ell_u^2} = \frac{[< h^2 >_o / M]m_o}{\ell_u^2} \qquad (2.4.1)$$

where $\langle h^2 \rangle_o$, the unperturbed (in theta condition, $A_2=0$) mean-square end-to-end distance; N, the number of main chain bonds of length $\ell_u$; M, the molar mass of the polymer; and $m_o$, the average mass per main chain bond. The value of $C_\infty$ is a quantitative measure of the effect of hindered rotation about the main chain bonds and fixed bond angles on $\langle h^2 \rangle$. For a freely jointed chain, which has neither rotational hindrance nor bond angle restrictions, $\langle h^2 \rangle$ is equal to $N\ell_u$[9-10]. Thus, a value of $C_\infty$ is equal to 1 for freely jointed chain, and larger $C_\infty$ values indicates that the polymer is less flexible.

The relative contributions of fixed angles can be elucidated by modification of freely jointed chain model. Erying[11] showed that when N is very large $\langle h^2 \rangle$ can be calculated as

$$\langle h^2 \rangle = (N\ell_u^2)\left(\frac{1+\cos\theta_1}{1-\cos\theta_1}\right) \qquad (2.4.2)$$

where $\theta_1$ is equal to 180° minus the fixed bond angle. Thus, for polyethylene backbone $\cos\theta = 0.333$ and $\langle h^2 \rangle = 2N\ell_u^2$ with fixed tetrahedral bond angles for a saturated hydro- carbon backbone being expected to double $\langle h^2 \rangle$.

In light of above, an alternative chain flexibility parameters, which is commonly used, is the conformation (steric) factor $\sigma$

$$\sigma = (\langle h^2 \rangle_o^{1/2})(\langle h^2 \rangle_f^{1/2})^{-1} \qquad (2.4.3)$$

which is obtained from the experimental $\langle h^2 \rangle_o$ value (measured in theta condition) and the $\langle h^2 \rangle$ value calculated from freely rotating chain i.e., $\langle h^2 \rangle_f$. $\sigma$ provides a measure of the relative increase in end-to-end distance brought about by hindrances to rotation only. Obviously, $C_\infty$ and $\sigma$ are related for tetrahedral hydrocarbon backbones by

$$C_\infty = 2\sigma^2 \qquad (2.4.4)$$

The effect of restricted rotation can be taken into account by introducing an additional term into eqn.(2.4.2). If the hindering potentials are mutually independent for neighboring bonds and symmetrical,[12-14] $<h^2>$ becomes

$$< h^2 > = (N\ell_u^2)\left(\frac{1+\cos\theta}{1-\cos\theta}\right)\left(\frac{1+ < \cos\phi >}{1- < \cos\phi >}\right) \qquad (2.4.5)$$

Here $<\cos \phi>$ is the average rotation angle ($\phi = 0$ for trans).

From eqn. (2.4.1), the evaluation of characteristic ratio requires measurement of the unperturbed dimensions of the polymer chain. Two common techniques for measuring unperturbed dimensions are laser light scattering and viscometric measurements on dilute polymer solutions. Macromolecular dimensions in solution are effected by both long range (excluded volume) and short range, which are the bond angle restriction and hindered rotation. In thermodynamically good solvents, where solvent/polymer-segment interactions are favored, the chain will expand to enhance these interaction and minimize polymer/ polymer interactions, namely "excluded volume effect". Conversely, in a thermodynamically poor solvent the chain will contract to minimize unfavorable polymer/solvent interactions. Flory[15] predicted that for polymer chain in dilute solution there would be exist an ideal or unperturbed state at which the so-called theta ($\theta$) condition. Here, through a appropriate choice of solvent and temperature, the chain segments to interact with other chain segments and with solvent is balanced (at that time, the second virial coefficient $A_2$ is equal to zero). Flory suggested that polymer chains in solution is at the theta condition and those in the bulk amorphous state should exhibit, at least approximately, identical conformations.

In light scattering, unperturbed dimensions is easily measured. By measuring a dilute solutions of a polydisperse polymer, the weight average molar mass $M_w$, the root mean square z-average radius of gyration $< R_g^2 >_z^{1/2}$, and the second virial coefficient $A_2$, which is a thermodynamic interactions, can be probed by using eqn. (2.1.29). If $A_2$ is equal to zero then the value of $<R_g^2>_z$ will be $< R_g^2>_{oz}$, that is the unperturbed value. Molar mass heterogeneity is an important consideration here, since the use of eqn. (2.1.29) for polydisperse material will give a weight average molar mass, $M_w$, but a z-average size $<R_g^2>_z$. Thus, in working with polydisperse materials it is important to correct for polydispersity effects.

However, laser light scattering experiments are not conducted under theta conditions. This may be because theta conditions are not known or because of the great ease associated with conducing light scattering measurements in good solvents. Baumann proposed[16] an equation to find out $<R_g^2>_0$

$$(< R_g^2 > /M)^{3/2} = (< R_g^2 >_o /M)^{3/2} + BM^{1/2} \qquad (2.4.6)$$

where B is the excluded volume parameter. Eqn. (2.4.6) suggests that $<R_g^2>_o/M$ may be evaluated by extrapolating good solvent values $(<R_g^2>_o/M)^{3/2}$ versus $M^{1/2}$ to $M^{1/2}$ =>0. Experiments have shown that eqn. (2.4.6) cannot be applied to those chains with high excluded volumes. Once $<R_g^2>_o$ is calculated by eqn. (2.4.6), $<h^2>_o$ can be transformed by

$$< h^2 >_o = 6 < R_g^2 >_o \qquad (2.4.7)$$

Hence, $C_\infty$ can be obtained via eqn. (2.4.1). It should be noted that eqn. (2.4.7) is valid in the case of the coil conformation.

**2.4.2 Stiff chains:** The Kratky-Porod wormlike chain model[17-18] is widely used for describing conformational characteristics of less flexible chains. The polymer is

viewed as a semi-flexible (or worm) of overall "contour length" L with a continuous curvature. The chain is divided into N segments of length $\Delta L$, which are linked at a supplementary angle $\psi$. The persistence length q ( Figure 2.4.1) is defines as[19]

$$q = \lim_{\psi \to 0, \Delta L \to 0} \frac{\Delta L}{1 - \cos \psi} \qquad (2.4.8)$$

and is thus a measure of the tendency for segments in the polymer chain to "remember" the orientation of adjoining and other segments in the chain. Wormlike chains will exhibit conformations ranging between random coil and rigid rods depending on the ratio of L/q. Therefore, q provides a measure of chain stiffness. Furthermore, it can be shown that at large L a wormlike chain becomes Gaussian and q is related to the mean square average end-to-end distance

$$q = \langle h^2 \rangle / 2L \qquad (2.4.9)$$

As with flexible chains, most studies of conformational behaviour of stiff chains have involved light scattering and intrinsic viscosity studies of dilute polymer solutions. Excluded volume effects are not significant for stiffer chains, so measured persistence lengths usually show slightly dependence on the solvent. However, the excluded volume effects become measurable when chain are very long ($L \geq 100\ q$) because it is easier for one segment to touch the others in the same polymer chain. Thus, the choice of solvent is normally of less importance in studying the conformation of stiff chains than it is for flexible ones. Benoit and Dotty[20] have related q and $\langle R_g^2 \rangle$ by the equation

$$\langle R_g^2 \rangle = q^2 [1/3(L/q) - 1 + (2q/L) - (2q^2/L^2) [1 - \exp( - L/q)]] \qquad (2.4.10)$$

Hence, measurement of $\langle R_g^2 \rangle$ by light scattering leads directly to q.

## 2.5 Calibration between translational diffusion coefficient D and molar mass M

**2.5.1 Conversion between Line-Width and Molar Mass Distributions:** It is well-known in polymer science that for the first-order approximation the translational diffusion coefficient D can be related to molecular weight M by[21]

$$D = k_D M^{-\alpha_D} \tag{2.5.1}$$

where $k_D$ and $\alpha_D$ are two scaling constants whose values depend mainly on polymer chain conformation and solvent quality. For a flexible polymer chain, $0.5 < \alpha_D < 0.6$ in a good solvent and $\alpha_D = 0.5$ in a Flory $\Theta$ solvent; for a rigid rod-like chain, $\alpha_D = 1$; and for a semi-rigid worm-like chain, $0.6 < \alpha_D < 1$. According to the definition, in dynamic LLS,

$$\left[g^{(1)}(t)\right]_{t\to 0} = < E(t)E^*(0) >_{t\to 0} = \int_0^\infty G(\Gamma)d\Gamma \propto < I > \tag{2.5.2}$$

where $<I>$ ($= <I>_{solution} - <I>_{solvent}$) is the net average scattering intensity. On the other hand, in static LLS, when $C \to 0$, and $q \to 0$,

$$R_{vv}(q \to 0) \propto <I> \propto M_w \propto \int_0^\infty f_w(M)M\, dM \tag{2.5.3}$$

where $f_w(M)$ is a differential weight distribution. A comparison of Eqs. (2.5.2) and (2.5.3) leads to

$$\int_0^\infty G(\Gamma)\ d\Gamma \propto \int_0^\infty f_w(M)\, M\ dM \tag{2.5.4}$$

where $G(\Gamma) \propto G(D)$ and $d\Gamma \propto dD$ because $\Gamma = Dq^2$. Therefore, Eqn. (2.5.4) can be rewritten as

$$\int_0^\infty G(D)\frac{dD}{dM}\ dM \propto \int_0^\infty f_w(M)\, M\ dM \tag{2.5.5}$$

On the basis of Eqn. (2.5.1), we can rewrite Eqn. (2.5.5) as

$$f_w(M) \propto \frac{G(D)}{M}\frac{dD}{dM} \propto G(D)D^{1+\frac{2}{\alpha_D}} \qquad (2.5.6)$$

where all proportional constants have been omitted because they are irrelevant to a given distribution. According to Eqs. (2.5.1) and (2.5.6), the values of $k_D$ and $\alpha_D$ are needed to transform D to M and G(D) to $f_w(M)$.

It should be emphasized once more that the molar mass distribution obtained in this way will be an estimate of the real molar mass distribution because dynamic laser light scattering is not a fractionation method and the Laplace inversion is not unique especially when the noise level in the measured time correlation function is high. Even with a number of recently developed excellent Laplace inversion programs, this is still an experimental problem, not a mathematical one. This is why it is crucially important to get a clean ("dust-free") solution before a laser light scattering measurement. Experimentally, we have to try our best to clarify the solution to ensure that the relative difference between the measured and calculated baselines is no more than 0.1%.

**2.5.2 Using a Set of Narrowly Distributed Standards:** The most straightforward calibration method would be to measure both D and M of a set of monodisperse samples with different molecular weights. Actually, in a real experiment, the monodisperse samples have to be replaced by a set of narrowly distributed standards made either directly from special polymerization methods or indirectly from the fractionation of a broadly distributed sample. However, it should be noted that only a few kinds of polymers, e.g., polystyrene and poly(methyl methylacrylate), can be directly made with a narrow molecular weight distribution ($M_w/M_n \sim 1.1$). On the other hand, the fractionation is very time consuming, if not impossible. Thus, the

application of this straightforward method is very limited in practice. Therefore, special analytical methods have to be developed to calibrate or scale the translational diffusion coefficient D and molar mass M from broadly distributed samples.

**2.5.3 Using Two or More Broadly Distributed Samples:**[22] It has been shown that a combination of static and dynamic laser light scattering can establish a calibration between D and M from two or more broadly distributed samples. The principle is outlined as follows. According to the definition of $M_w$ and on the basis of Eqs. (2.5.1) and (2.5.6), we have

$$M_{w,calcd}^{DLS} = \frac{\int_o^\infty F_w(M)M\ dM}{\int_o^\infty F_w(M)\ dM} = \frac{k_D^{1/\alpha_D}\int_0^\infty G(D)dD}{\int_0^\infty G(D)D^{1/\alpha_D}dD} = \frac{k_D^{1/\alpha_D}}{\int_0^\infty G(D)D^{1/\alpha_D}dD} \qquad (2.5.7)$$

where we have used the normalization condition: $\int_0^\infty G(D)dD = 1$. On the basis of eqn. (2.5.7), for two samples 1 and 2, we have

$$\frac{(M_{w,calcd}^{DLS})_1}{(M_{w,calcd}^{DLS})_2} = \left[\int_0^\infty G_2(D)D^{1/\alpha_D}dD\right] / \left[\int_0^\infty G_1(D)D^{1/\alpha_D}dD\right] \qquad (2.5.8)$$

For a given polymer sample, $M_{w,calcd}^{DLS}$ calculated on the basis of G(D) from dynamic LLS should equal to $M_{w,measd}$ measured directly from static LLS. It is expected that a proper choice of $\alpha_D$ should lead to a minimum difference between $[(M_{w,1})/(M_{w,2})]_{calcd}$ and $(M_{w,1})/(M_{w,2})]_{measd}$, which is actually done by iterating $\alpha_D$ in a computer program.

## 2.6 Calibration by off-line GPC, Static and Dynamic LLS

Using static laser light scattering apparatus as an on-line GPC detector has been known for a while. Here, we intend to illustrate a less known method of combining the GPC and LLS results. The basic principle is as follows:

There is a similarity between dynamic light scattering and gel permeation chromatography (GPC), namely both the translational diffusion coefficient D obtained in dynamic LLS and the elution volume V measured in GPC are related to the hydrodynamic size, or the molar mass, of a given macromolecular sample. For the first-order approximation,

$$V = A + B \log(M) \tag{2.6.1}$$

where $A$ and $B$ are two calibration constants similar as $k_D$ and $\alpha_D$. It should be noted that the first-order approximation will simplify, but not affect, the following discussion: A combination of eqs. (2.5.1) and (2.6.1) leads to

$$V = \boldsymbol{A} + \boldsymbol{B} \log(D) \tag{2.6.2}$$

where $\boldsymbol{A} = A + B \log(k_D)/\alpha_D$ and $\boldsymbol{B} = -B/\alpha_D$. Further, by taking the square of both sides of eqn. (2.6.2), we have

$$V^2 = \boldsymbol{A}^2 + 2\boldsymbol{AB} \log(D) + \boldsymbol{B}^2 \log^2(D) \tag{2.6.3}$$

After integrating both sides of eqs. (2.6.2) and (2.6.3), we have

$$\langle V \rangle = \boldsymbol{A} + \boldsymbol{B} \langle \log(D) \rangle \tag{2.6.4}$$

and

$$\langle V^2 \rangle = \boldsymbol{A}^2 + 2\boldsymbol{AB} \langle \log(D) \rangle + \boldsymbol{B}^2 \langle \log^2(D) \rangle \tag{2.6.5}$$

where

$$\langle V \rangle = \int_0^\infty VC(V)\ dV \quad \text{and} \quad \langle V^2 \rangle = \int_0^\infty V^2 C(V)\ dV \tag{2.6.6}$$

which can be calculated directly from C(V), and

$$\langle \log(D) \rangle = \frac{\int_0^\infty \log(D) C(V)\ dV}{\int_0^\infty C(V)\ dV}$$

and

$$\langle \log^2(D) \rangle = \frac{\int_0^\infty \log^2(D) C(V)\, dV}{\int_0^\infty C(V)\, dV} \tag{2.6.7}$$

On the other hand, since C(V) is a weight (or concentration) distribution, we have

$$\int_0^\infty C(V)dV \propto \int_0^\infty f_w(M)dM \propto \int_0^\infty f_w(M)Md[\log(M)] \tag{2.6.8}$$

Using $dV \propto d[\log(M)] \propto d[\log(D)]$ and eqn. (2.6.8), we have

$$C(V) \propto f_w(M)M \propto G(D)D^{1+\frac{1}{\alpha_D}} \tag{2.6.9}$$

so that eqn. (2.6.7) can be rewritten as

$$\langle \log(D) \rangle = \frac{\int_0^\infty \log(D) G(D) D^{1/\alpha_D} dV}{\int_0^\infty G(D) D^{1/\alpha_D} dV}$$

and

$$\langle \log^2(D) \rangle = \frac{\int_0^\infty \log^2(D) G(D) D^{1/\alpha_D} dV}{\int_0^\infty G(D) D^{1/\alpha_D} dV} \tag{2.6.10}$$

Using eqn. (2.6.9), we can calculate $M_w$ from C(V) by

$$M_{w,calcd}^{SEC} = \frac{\int_0^\infty F_w(M)MdM}{\int_0^\infty F_w(M)dM} = k_d^{1/\alpha_D} \int_0^\infty 10^{(\mathbf{A}-V)/(\alpha_D \mathbf{B})} C(V)dV \tag{2.6.11}$$

where we have used $\int_0^\infty C(V)dV = 1$. For a given polymer sample, $M_{w,calcd}^{SEC}$ should be equal to $M_{w,calcd}^{DLS}$, i.e., on the basis of eqs. (2.5.7) and (2.6.11), we have

$$\left[\int_0^\infty 10^{(\mathbf{A}-V)/(\alpha_D \mathbf{B})} C(V)\, dV\right]\left[\int_0^\infty G(D) D^{1/\alpha_D} dD\right] = 1 \tag{2.6.12}$$

This is only one unknown parameter $\alpha_D$ in eqn. (2.6.12). For a chosen $\alpha_D$, we can *first* calculate $\langle \log(D) \rangle$ and $\langle \log^2(D) \rangle$ using eqn. (2.6.7); then solve **A** and **B** on the basis of eqs. (2.6.4) and (2.6.5); and finally calculate the left side of eqn. (2.6.12). By iterating $\alpha_D$, we can find a proper value of $\alpha_D$ which minimizes the difference between

the left and right sides of eqn. (2.6.12). With this $\alpha_D$, we can calculate $k_D$ from either eqn. (2.5.7) or (2.6.11) by using $M_w$ determined directly from static LLS and G(D) from dynamic LLS or C(V) from SEC. With **A**, **B**, $k_D$ and $\alpha_D$, we are ready to calculate *A* and *B*. In this way, we can calibrate not only M with V, but also M with D in one single process with only one broadly distributed sample.

## 2.7 References


1 Zimm, B.H. *J. Chem. Phys.* **1948**, *16*, 1099.

2 Chu, B. *Laser Light Scattering,* 2nd Ed, Academic Press, New York **1991**.

3 Stockmayer, W. H.; Schmidt, M. *Pure & Appl. Chem.* **1982,** *54*, 407.

4 Stockmayer, W. H.; Schmidt, M. *Macromolecules* **1984,** *17,* 509.

5 Munk, P. *Introduction to macromolecular science*; John Wiley & Sons, Inc.: Singapore, 1989

6 Xu, Z.; Hadjichristidis, N.; Fetters, L. J.; Mays, J. W. in Advances in Polymer Science; Springer: New York, 1995, 120, p1-50.

7 Flory, P.J. *Statistical mechanics of chain molecules Interscience*; New York, 1969

8 Flory, P.J. *Macromolecules* **1974**, *7*, 381

9 Kuhn, W. **1983**, *Kolloid-Z* **1934**, 86, 2 *Kolloid-Z* **1936**, 76, 258 *Kolloid-Z* **1939**, *87*, 3.

10 Guth, E.; Mark, H. *Monstach Chem* **1934,** *65*, 93.

11 Eyring H *Phys Rev* **1932,** *39*, 746.

12 Benoit, H. *J Chem Phys* **1947**, *44*, 18.

13 Kuhn. H. *J Chem Phys* **1947,** *15*,843.

14 Taylor, W.J. *J Chem Phys* **1948**, *16*, 257.

15 Flory, P.J. *Principles of polymer Chemistry*, Cornell University Press, Ithaca, NY, 1953, pp423-426.

16 Baumann, H. *J Polym Sci, Polym Lett* **1965**, *3*, 1069.

17 Kratky, O.; Porod, G. *Recl Trav Chim* **1949**, *68*, 1106.

18 Porod, G. *Monatsh. Chem* **1949**, *2*, 251.

19 Fujita, H. *Polymer solutions*. Elsevier, Amstardam, 1990, p140.

20 Benoit, H.; Dotty, P. *J of Phys Chem.* **1953**, *57*, 958.

21 de Gennes P.G. *Scaling Concepts in Polymer Physics*, Cornell University Press,1979

22 Wu, C.; Zhang, Y.B.; Yan, X.H.; Cheng, R.S. *Acta Polymerica Sinica* **1995**, *3*, 349

# Chapter 3

# Experimental

## 3.1 Laser Light Scattering Instrumentation

A modified commercial light-scattering spectrometer (ALV/SP-125) equipped with an ALV-5000 multi-τ digital time correlator and an solid state laser for the characterization of polyimides (ADLAS DPY 425II, output power ≈ 400 mW at $\lambda_o$ = 532.8 nm) or with an Helium neon laser for the characterization of polyarylenes and poly(aryleneethnylene)s (Spectra-Physics 127, operated at a wavelength of 632.8 nm and output power ≈ 25 mW) as the light source (Figure 3.1.1) was used. By this spectrometer, both static and dynamic light scattering measurement can be done. The primary beam is vertically polarized. A compensated beam attenuator (Newport M-925B) was used to regulate the incident laser light intensity to avoid possible localized heating in the light-scattering cuvette. The cell contained dust free sample solution was put in the index matching vat, in which the temperature is controlled by NESLAB RTE-210 refrigerated bath/circulator. The intensity of scattered light was detected by THORN EMI photomultiplier tube for counting the number of photons. In static LLS, the instrument was calibrated with toluene to make sure that the scattering intensity from toluene has no angular dependence in the range of 15° - 150°. The intensity-intensity time correlation functions (dynamic LLS) were measured by an ALV-5000 multiple-τ digital correlator. The correlation functions were accumulated until the net photon count was beyond $10^6$ per second. The difference between the measured and calculated baselines was no more than 0.1%. The LLS measurements were carried out

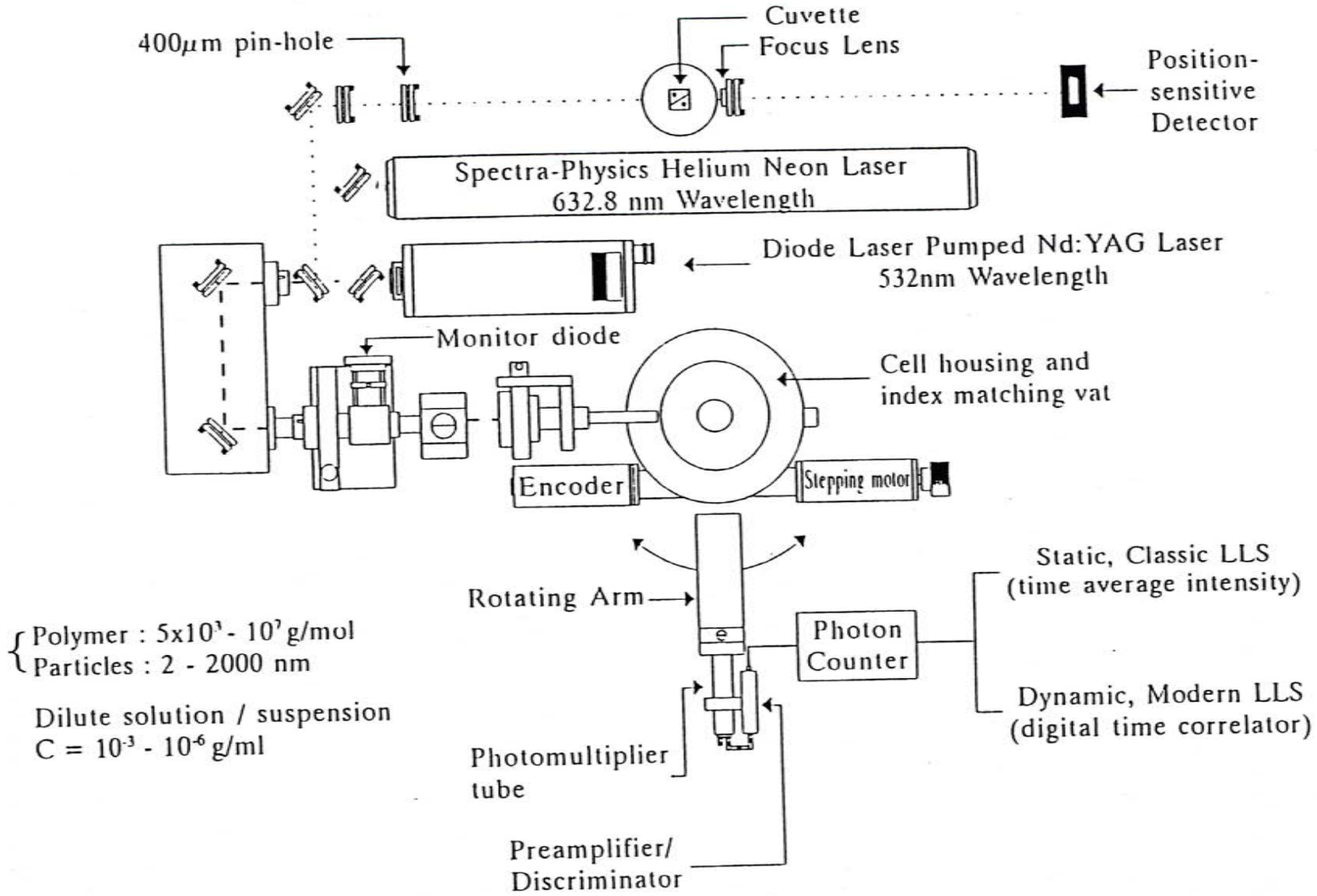


Figure 3.1.1 : ALV-5000 Laser Light Scattering Spectrometer incorporated with differential refractometer

at 25.0 ± 0.1 and 30.0 ± 0.1 °C for polyarylenes and poly(aryleneethnylene)s, and polyimides respectively.

### 3.2 Refractive index increment measurement

All specific refractive index increments (dn/dc) were determined by a recently developed differential refractometer[1]. In this novel refractometer, a small pinhole with a diameter of 400 μm is illuminated with a laser light (Figure 3.1.1). The illuminated pinhole is imaged to a 6 mm position-sensitive detector (Hamamatsu S3932) by a lens located in equal distance between the pinhole and the detector. The distance between the detector and the pinhole is four times the focal length (f = 10 cm) of the lens, i.e., a (2f - 2f) optical design have been used instead of a conventional (1f) design where a parallel incident light beam is used, and the distance between the detector and the lens is only one focal length. This (2f-2f) design is optically equivalent to placing the detector directly behind the pinhole, so that the laser beam drift is eliminated. A refractometer cuvette (Hellma 590.049-QS, with 60° partition to two chambers) is placed just in front of the lens. The pinhole, the cuvette, the lens, and the detector are rigidly mounted on a small optical rail. The refractometer has dimensions of only 40 cm in length, 15 cm in width, and 10 cm in height. The output voltage of the detector is proportional to the displacement of the light spot from the center of the detector caused by the refractive index difference between the polymer solution and the solvent. The detector resolution is 0.2μm, which corresponds to resolution of $10^{-6}$ in the refractive index measurement. This refractometer has been incorporated into the laser light-scattering spectrometer, wherein the same laser has been used as the light sources in both the laser light-scattering spectrometer and

differential refractometer. Thus, the problem of wavelength correction is eliminated. In comparison with a conventional differential refractometer where a micrometer is normally used to read the beam displacement, the use of the position-sensitive detector together with the data acquisition system (a 16-bit analog-to-digital data acquisition card (National Instrument)) not only increases the accuracy of measured $\upsilon$ but also makes a large amount of measurements possible and easier. The temperature of the cuvette was precisely controlled by YSI Proportional Temperature Controller (Model 72).

For each measurement, the reading of the position-sensitive detector was set zero by filling both sides of the cuvette chambers with solvent. Afterward, the solution was filled into the solution chamber, and then the difference in the refractive index ($\Delta n$) between the solution and solvent was recorded. After each measurement, both sides of the cuvette was filled with solvent to check the zero point. The value of dn/dC was obtained from the slope of the graph of $\Delta n$ against concentration of the sample.

### 3.3 Gel permeation chromatography

Polyarylenes and poly(aryleneethynylene)s were also characterized by the GPC. One Ultrastyragel 500A (7.8 x 300 mm, Part no. 10571) and two Ultrastyragel linear (7.8 x 300 mm, Part no. 10681) GPC columns calibrated by polystyrene standards together with a Waters 510 HPLC Pump and a Waters 410 Differential Refractometer were used. THF was used as eluent and the flow rate was 1.23 mL/min. The concentration of the samples are ca. 2 - 5 mg polymer in 5 mL THF. The temperature of the columns was kept at 40 °C.

## 3.4 References

1. Wu, C.; Xia, K. Q. *Rev. Sci. instrum.* **1994**, *65* (3), 587

# Chapter 4

## Laser Light Scattering Studies of Soluble High Performance Fluorine-containing Polyimides

### 4.1 Introduction

Aromatic polyimides have been being widely used in making films, coatings, fibers and adhesives due to their high thermal stability and excellent mechanical properties[1,2]. Recently, polyimides with low dielectric constant, low water absorption and low thermal expansion have been applied to electronic devices[3]. Therefore, investigating microscopic parameters of polyimide chains is very important to the development of more advanced polyimide related materials..

However, it is hard to dissolve polyimides in common organic solvents because of their chain stiffness, which hinders the study of their solution properties. In the past, the molecular parameters of insoluble polyimides had to be estimated from their precursors, i.e., from polyamic acid formed in the first stage of the reaction between diamines and anhydrides. The estimation has some problems, such as the polyelectrolytes effect in the precursor solution and the structure discrepancy between the precursor and final polymer[4,5].

Recently, soluble high performance polyimides have been developed[6,7]. The dissolution is achieved by introducing some side groups, such as $-CH_3$ and $-CF_3$, in the polymer chain to twist the aromatic imide rings and the phenyl groups in order to decrease the chain-to-chain interaction. In addition, some joints, such as -O- and $-CH_2-$, are used to separate the aromatic imide rings and the phenyl rings so as to

increase the chain flexibility. Recent investigations have shown that introducing the fluorinated groups, the refractive index, water absorption and dielectric constant of polyimides are significantly reduced[8-10], which is important to the development of electronic devices.

In this study, two kinds of polyimides, 6FDA-PFMB and HFBPDA-PFMB, were made individually by a one-step polycondensation of 2,2'-bis(3,4'-dicarboxyphenyl)hexafluoro-propane dianhydride (6FDA) and 2,2'-(trifluoromethyl)-4,4'-diaminobiphenyl diamine (PFMB), and of 2,2'-bis(trifluoromethyl)-4,4',5,5'-biphenyltetracarboxylic dianhydride (HFBPDA) and 2,2'-(trifluoromethyl)-4,4'-diaminobiphenyl diamine (PFMB) respectively[11,12]. In comparison with the conventional two-step reaction, higher molar mass polyimides were obtained. The structure of 6FDA-PFMB and HFBPDA-PFMB are as follows:

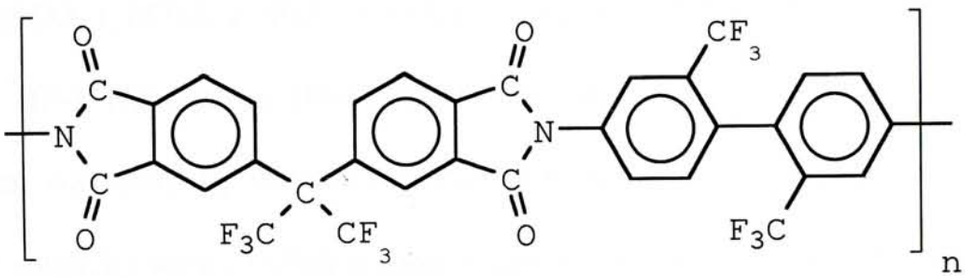

6FDA-PFMB

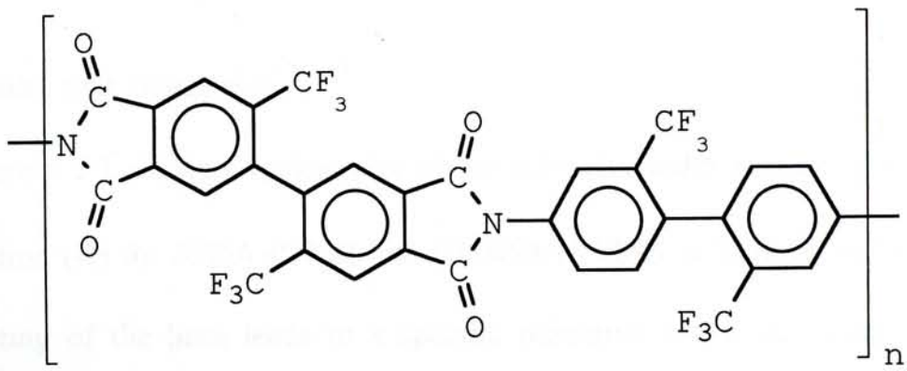

HFBPDA-PFMB

The backbone of these polyimides contain four trifluoromethyl groups, which

enhances their solubility in common organic solvents, such as tetrahydrofuran (THF) and methyl ethyl ketone (MEK).

## 4.2 Sample Preparation

Synthesis of 6FDA-PFMB and HFBPDA-PFMB has been described before[11,12]. Five 6FDA-PFMB and seven HFBPDA-PFMB fractions were obtained using a Waters Fraction Collector in conjunction with a Waters 150 CV chromatography system consisted of a series of four Waters Ultrastyragel columns in the order of $10^5$, $10^4$, $10^3$, and $10^2$ nm, wherein ACS regent grade THF was used as the mobile phase and the flow rate was 1.0 mL/min. The collected fractions were transferred into flasks to evaporate the solvent and were dried in vacuum for 24 hours at 125 °C prior to the experiments. According to the fractionation order, they were termed as, for 6FDA-PFMB: 6FDA-1, 6FDA-2, 6FDA-3, 6FDA-4 and 6FDA-5; for HFBPDA-PFMB: HF-1, HF-2, HF-3, HF-4, HF-5, HF-6 and HF-7 hereafter. Analytical reagent grade THF as solvent was dried by sodium and then distilled under nitrogen before use. All polymer solutions were clarified at room temperature using 0.5-μm PTFE membrane filter.

## 4.3 Results and Discussion

Figure 4.3.1 shows a typical plot of the refractive index increment (Δn) versus concentration (C) for 6FDA-PFMB and HFBPDA-PFMB in THF at 30 °C. A least-square fitting of the lines leads to a specific refractive index increment (dn/dC) = 0.182 ± 0.002 mL/g and 0.148 ± 0.002 mL/g for 6FDA-PFMB and HFBPDA-PFMB respectively at T = 30.0 °C and $\lambda_o$ = 532 nm. Eq. A.1.29 shows that both $M_w$ and $A_2$

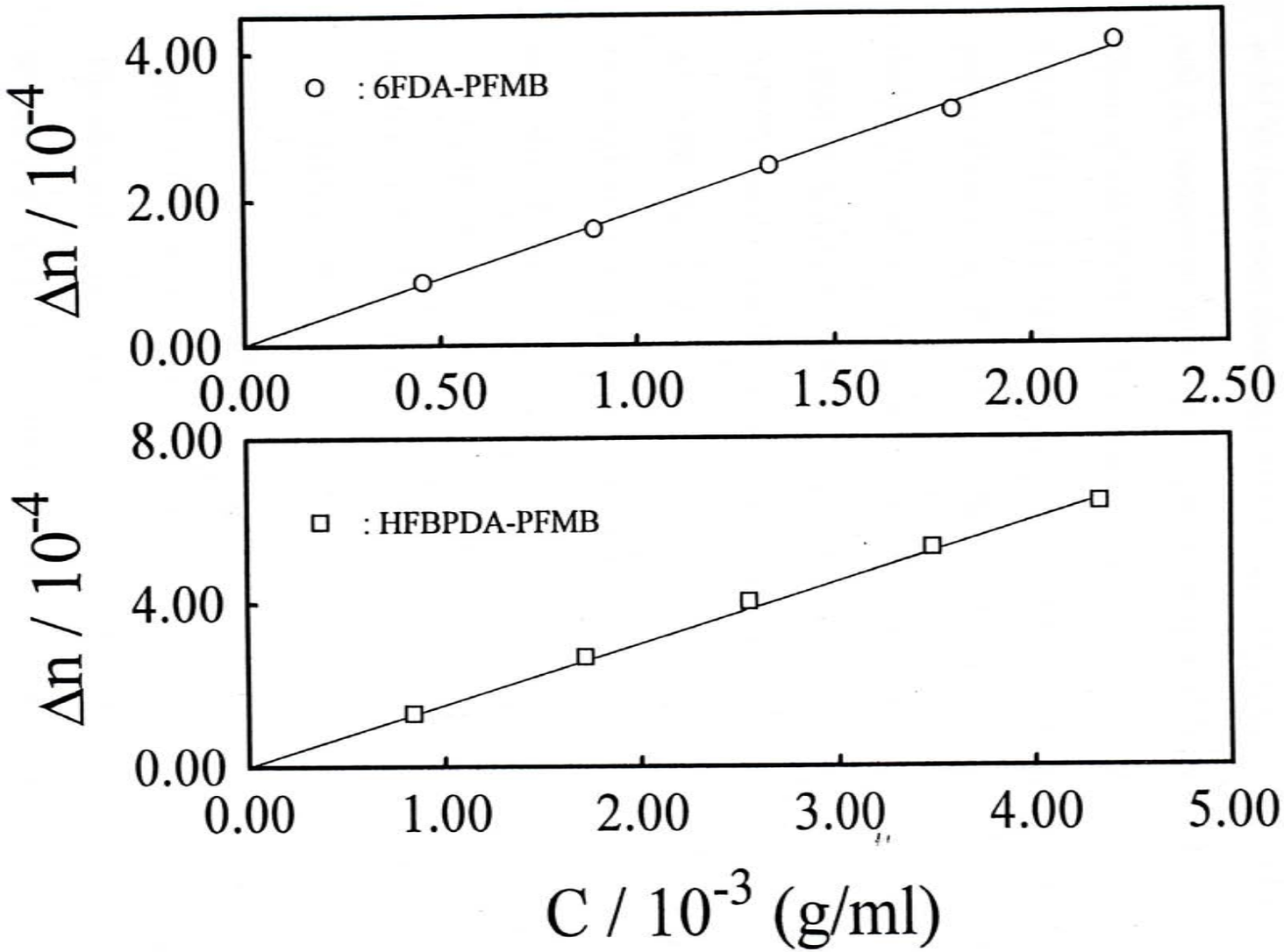


**Figure 4.3.1** Two typical plots of the refractive index increment (Δn) versus concentration (C) for the both polyimides in THF at T = 30 $^0$C and λ = 532 nm.

depend on the square of dn/dC, so that the accurate dn/dC value obtained in Figure 4.3.1 has ensured a good characterization of $M_w$ and $A_2$.

Figure 4.3.2 shows a typical Zimm plot for the both polyimides fractions in THF at 30 °C. From each Zimm plot, we were able to determine the values of $M_w$, $\langle R_g \rangle$ and $A_2$ respectively from the extrapolations of $[KC/R_{vv}(q)]_{c\to 0,\theta\to 0}$, $[KC/R_{vv}(q)]_{c\to 0}$ versus $q^2$ and $[KC/R_{vv}(q)]_{\theta\to 0}$ versus C. The static LLS results are summarized in Table 4.3.1. The positive $A_2$ values indicate that THF is a good solvent for the both polyimides at 30 °C. The 6FDA-1, 6FDA-2, HF-1, HF-2 and HF-3 chains are so short that $R_{vv}(\theta)$ practically shows no angular dependence and their $\langle R_g \rangle$ values cannot be accurately determined. The calibrations, for 6FDA-PFMB: $\langle R_g \rangle$ (nm) = 3.87 x $10^{-2}M_w^{0.568}$, and for HFBPDA-PFMB: $\langle R_g \rangle$ (nm) = 2.24 x $10^{-2}M_w^{0.626}$ were established where the $\langle R_g \rangle$ values of 6FDA-1, 6FDA-2, HF-1, HF-2 and HF-3 are estimated from their corresponding $\langle R_h \rangle$ values and their corresponding average value of the ratio $\langle R_g \rangle / \langle R_h \rangle$.

Figure 4.3.3 shows a typical measured intensity-intensity time correlation function for the both polyimides in THF at $\theta = 30°$ and T = 30 °C. It is known that for a polydisperse sample $g^{(1)}(t,q)$ is related to the line-width distribution $G(\Gamma)$ by eqn A.2.19. The Laplace inversion program CONTIN equipped with the correlator was used in this work to convert $G^{(2)}(t,q)$ to $G(\Gamma)$ on the basis of eqs. A.2.17 and A.2.19. The left insert in Figure 4.3.3 shows a typical $G(\Gamma)$. The line width $\Gamma$ usually depends on both C and q eqn A.2.20. The values of D, *f*, and $k_d$ respectively obtained from the plots $(\Gamma/q^2)_{c\to 0,\theta\to 0}$, $(\Gamma/q^2)_{c\to 0}$ versus $q^2$ and $(\Gamma/q^2)_{\theta\to 0}$ versus C are also listed in Table 4.3.1. No angular dependence of $(\Gamma/q^2)$ is observed in some low molecular weight fractions, implying that the values of $f\langle R_g^2 \rangle_z q^2$ is very small. This is understandable

**Table 4.3.1.** Summary of Static and Dynamic Laser Light-Scattering results of both polyimides fractions

| Sample | $10^{-4}$ $M_w$ (g/mol) | $\langle R_g \rangle$ (nm) | $10^4 A_2$ (mol·cm$^3$/g$^2$) | $10^8 \langle D \rangle$ (cm$^2$/s) | $k_d$ mL/g | $f$ | $\langle R_h \rangle$ (nm) | $\langle R_g \rangle / \langle R_h \rangle$ | $10^{-4}(M_w)_{calcd}$ (g/mol) | $M_z/M_w$ | $M_w/M_n$ |
|---|---|---|---|---|---|---|---|---|---|---|---|
| 6FDA-1 | 0.69 | ----- | 53.4 | 149 | ~0 | ~0 | 3.38 | ----- | 0.68 | 2.4 | 2.0 |
| 6FDA-2 | 1.54 | ----- | 23.0 | 94.8 | 13 | ~0 | 5.35 | ----- | 1.64 | 1.7 | 1.6 |
| 6FDA-3 | 5.99 | 17.4 | 28.2 | 48.2 | 27 | ~0 | 10.5 | 1.66 | 5.37 | 1.8 | 1.6 |
| 6FDA-4 | 13.4 | 32.4 | 11.2 | 28.1 | 41 | ~1 | 18.0 | 1.80 | 13.9 | 1.9 | 1.7 |
| 6FDA-5 | 20.3 | 41.9 | 10.3 | 22.4 | 75 | ~1 | 22.6 | 1.85 | 20.0 | 2.2 | 1.9 |
| HF-1 | 2.69 | ----- | 22.1 | 72.6 | 30 | ~0 | 6.99 | ----- | 2.63 | 1.9 | 1.7 |
| HF-2 | 3.30 | ----- | 14.2 | 61.7 | 29 | ~0 | 8.23 | ----- | 3.33 | 2.1 | 1.8 |
| HF-3 | 4.14 | ----- | 27.6 | 52.6 | 31 | ~0 | 9.63 | ----- | 4.24 | 2.0 | 1.8 |
| HF-4 | 5.35 | 20.7 | 13.9 | 44.8 | -26 | ~0 | 11.3 | 1.83 | 5.60 | 1.7 | 1.6 |
| HF-5 | 5.92 | 20.8 | 23.9 | 45.0 | 25 | ~0 | 11.3 | 1.84 | 5.44 | 1.9 | 1.7 |
| HF-6 | 6.41 | 23.3 | 20.4 | 40.7 | 80 | ~0 | 12.4 | 1.88 | 6.53 | 1.6 | 1.5 |
| HF-7 | 6.93 | 24.0 | 17.5 | 40.0 | 52 | ~0 | 12.7 | 1.89 | 6.84 | 1.4 | 1.4 |

The relative errors: $M_w$, ± 5 %; $\langle R_g \rangle$, ± 10-15 %; $A_2$, ± 15 %; $\langle D \rangle$, ± 3 %.

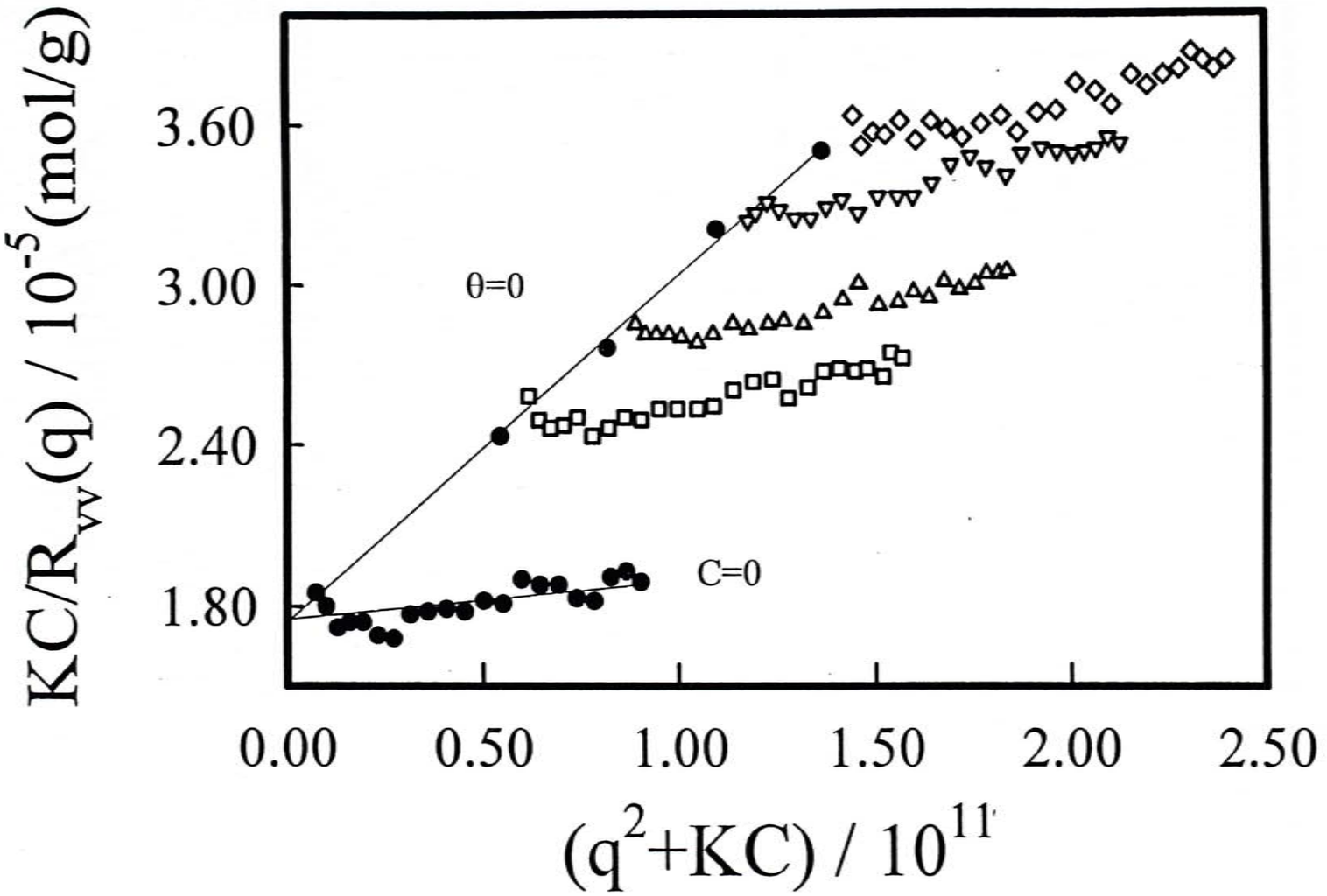


**Figure 4.3.2** A typical Zimm-plot of the polyimides fractions in THF at T = 30 °C, where the concentration of the polymer solution ranges from 0.4 x $10^{-3}$ g/ml to 2 x $10^{-3}$ g/ml.

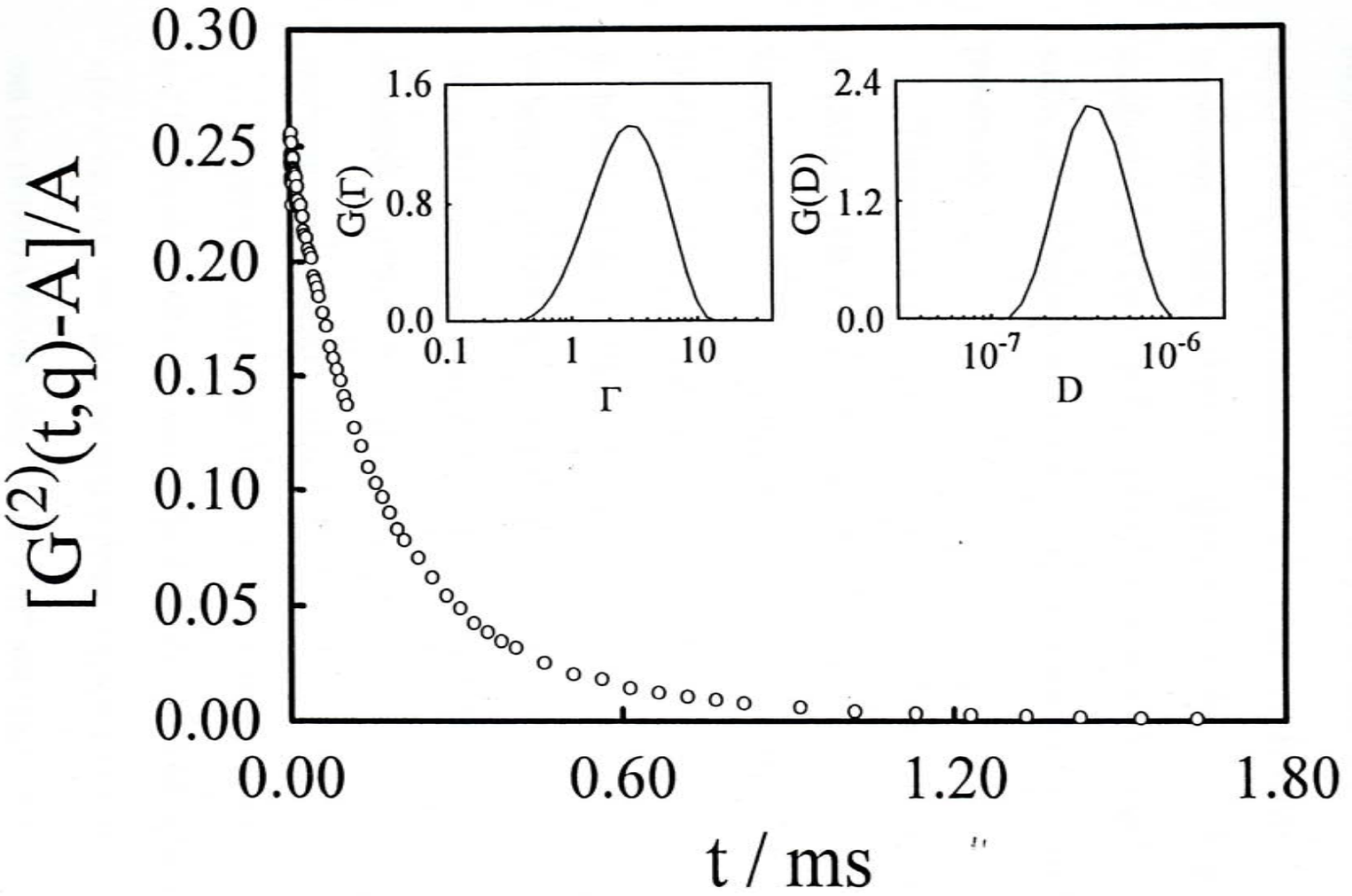


**Figure 4.3.3** A typical measured intensity-intensity time correlation function for the both polyimides in THF at $\theta = 30°$ and T = 30 °C. The left insert shows a corresponding line-width distribution G(Γ) calculated from $G^{(2)}(t,q)$. The right insert shows a corresponding translational diffusion coefficient distribution G(D) calculated from G(Γ).

because the size of polymers is so small that the contribution of internal motions to the relaxation is insignificant[13,14]. In a good solvent ($A_2 > 0$), $\Gamma/q^2$ is less dependent on C than $R_{vv}(\theta)$ because of a partial cancellation of the thermodynamic term $2A_2M_w$ by the hydrodynamic interaction ($C_DN_AR_h^3/M_w$). In the case of $C \sim 10^{-4}$ and $\theta < 30°$, $(1 + k_dC)(1 + f\langle R_g^2\rangle_z q^2) \sim 1$, so that $\Gamma/q^2 = D$ and $G(\Gamma)$ can be directly transformed into a translational diffusion coefficient distribution G(D) or a hydrodynamic radius distribution $f(R_h)$ using the Stokes-Einstein equation: $D \equiv kT/(6\pi\eta R_h)$, where k, T, and $\eta$, are the Boltzmann constant, the absolute temperature, and solvent viscosity, respectively.

The right insert in figure 4.3.3 shows a typical translational diffusion coefficient distributions G(D) of the both polyimides fractions in THF at T = 30°C. From each G(D), we were able to calculate a *z*-average translational diffusion coefficient $\langle D\rangle$ [$\equiv \int_0^\infty G(D)D\ dD$] and an average hydrodynamic radius $\langle R_h\rangle$ after replacing D in the Stokes-Einstein equation with $\langle D\rangle$. The values of $\langle D\rangle$, $\langle R_h\rangle$, and $\langle R_g\rangle/\langle R_h\rangle$ of both polyimides fractions are also summarized in Table 4.3.1. The ratio of $\langle R_g\rangle/\langle R_h\rangle$ are in the range of ~ 1.7 - 1.9, higher than ~ 1.5 predicted for monodisperse random coil chains[15], but close to ~ 1.84 predicted for random coil chains with a polydispersity index ($M_w/M_n$) of ~ 2.

Figure 4.3.4 shows log($\langle D\rangle$) is a linear function of log($M_w$.) of 6FDA-PFMB and HFBPDA-PFMB respectively. The solid lines represent a least-square fitting of $\langle D\rangle = \langle k_D\rangle M_w^{-\langle\alpha_D\rangle}$ with, for 6FDA-PFMB: $\langle k_D\rangle = 2.13 \times 10^{-4}$ and $\langle\alpha_D\rangle = 0.560$, and for HFBPDA-PFMB: $\langle k_D\rangle = 3.99 \times 10^{-4}$ and $\langle\alpha_D\rangle = 0.621$, where $\langle\ \rangle$ means that the values of $\langle k_D\rangle$ and $\langle\alpha_D\rangle$ were obtained from $\langle D\rangle$ and $M_w$ rather than from

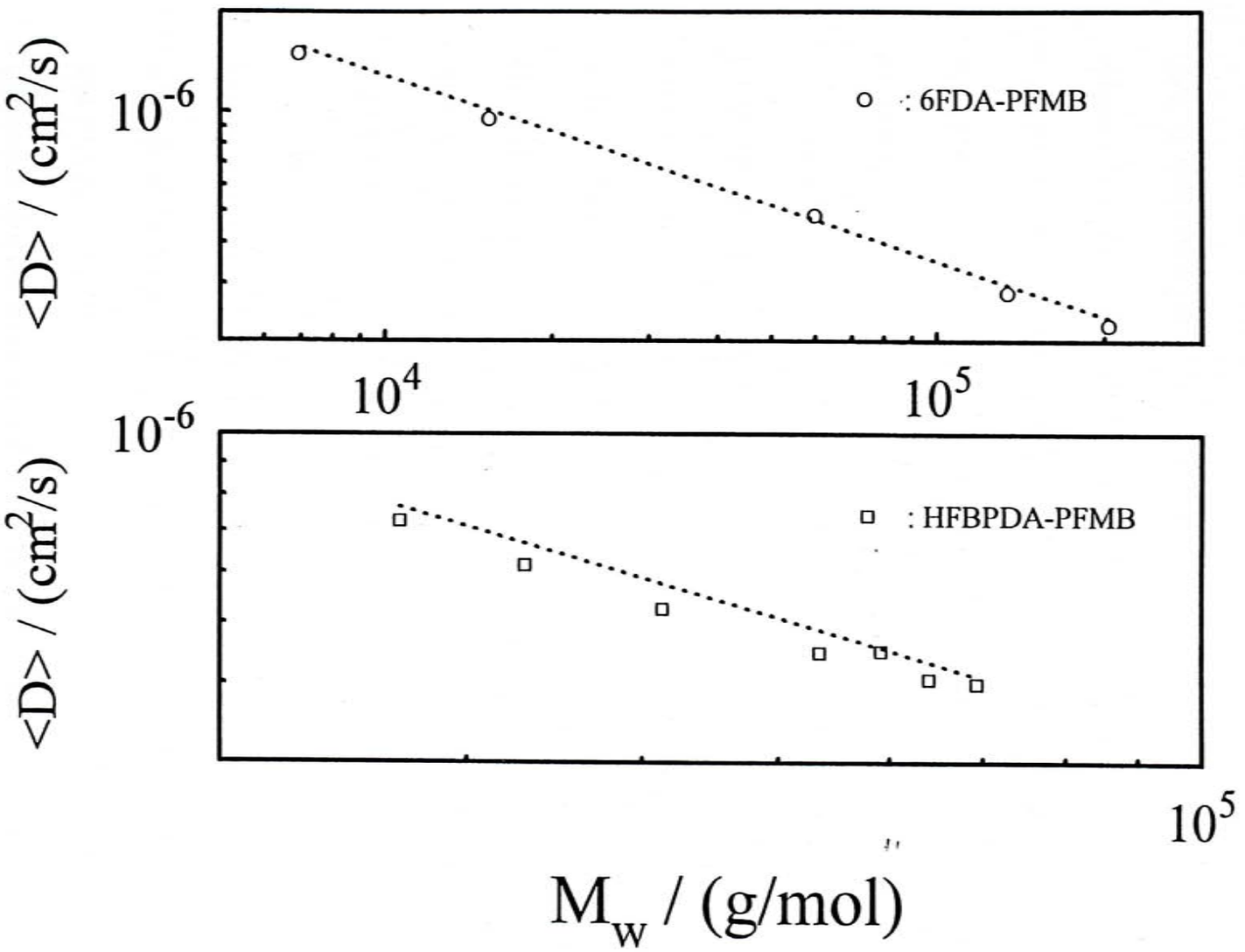


**Figure 4.3.4** For 6FDA-PFMB, the solid line represents the least-square fitting of <D> ($cm^2/s$) = 2.13 x $10^{-4}M_w^{-0.560}$; and the dotted line, D ($cm^2/s$) = 2.41 x $10^{-4}M^{-0.564}$ for monodisperse species. For HFBPDA-PFMB, the solid line represents the least-square fitting of <D> ($cm^2/s$) = 3.99 x $10^{-4}M_w^{-0.621}$; and the dotted line, D ($cm^2/s$) = 6.16 x $10^{-4}M^{-0.656}$ for monodisperse species.

D and M for monodisperse species. The value of $<\alpha_D>$ of HFBPDA-PFMB is greater than that of 6FDA-PFMB which means that the HFBPDA-PFMB chains in THF at T = 30 °C has a more extended conformation.

Knowing $k_D$ and $\alpha_D$, we can calculate $M_w$ by eqn 2.5.7 from G(D) in dynamic LLS. If approximating $k_D$ and $\alpha_D$ with $<k_D>$ and $<\alpha_D>$, we found that the calculated values of $M_w$ of both polyimides fractions are much smaller than the values of $M_w$ directly measured in static LLS. This disagreement is understandable because $<k_D> \neq k_D$ and $<\alpha_D> \neq \alpha_D$ for the moderately distributed 6FDA-PFMB and HFBPDA-PFMB fractions.

Section 2.5.3 has shown a method of combining static and dynamic LLS results to obtain $k_D$ and $\alpha_D$ from the measured values of $M_w$ and G(D). Using this combination method, we found that, for 6FDA-PFMB: $k_D = 2.41 \times 10^{-4}$ and $\alpha_D = 0.564$, and for HFBPDA-PFMB: $k_D = 6.16 \times 10^{-4}$ and $\alpha_D = 0.656$. These pairs of $k_D$ and $\alpha_D$ define the calibrations between D and M for monodisperse 6FDA-PFMB and HFBPDA-PFMB in THF at T = 30 °C, shown in Figure 4.3.4 by the dotted line. With this pair of $k_D$ and $\alpha_D$, we converted each G(D) to a corresponding $f_w(M)$.

Figure 4.3.5 and 4.3.6 show molar mass distributions $f_w(M)$ of five 6FDA-PFMB and seven HFBPDA-PFMB fractions. From each $f_w(M)$, we calculated a corresponding weight-average molar mass $(M_w)_{calcd}$ and polydispersity index $M_w/M_n$ and $M_z/M_w$ ,which are also listed in Table 4.3.1. The calculated values of $(M_w)_{calcd}$ agree well with the measured values of $M_w$ from static LLS. The values of $M_w/M_n \leq 2$ are expected since the both polyimides were made by polycondensation. We can estimate the persistence length ($q$) on the basis of Kratky-Porod wormlike chain model by the eqn 2.4.10. In the equation, L ($= n\ell_u$) is the contour length with $\ell_u$ being

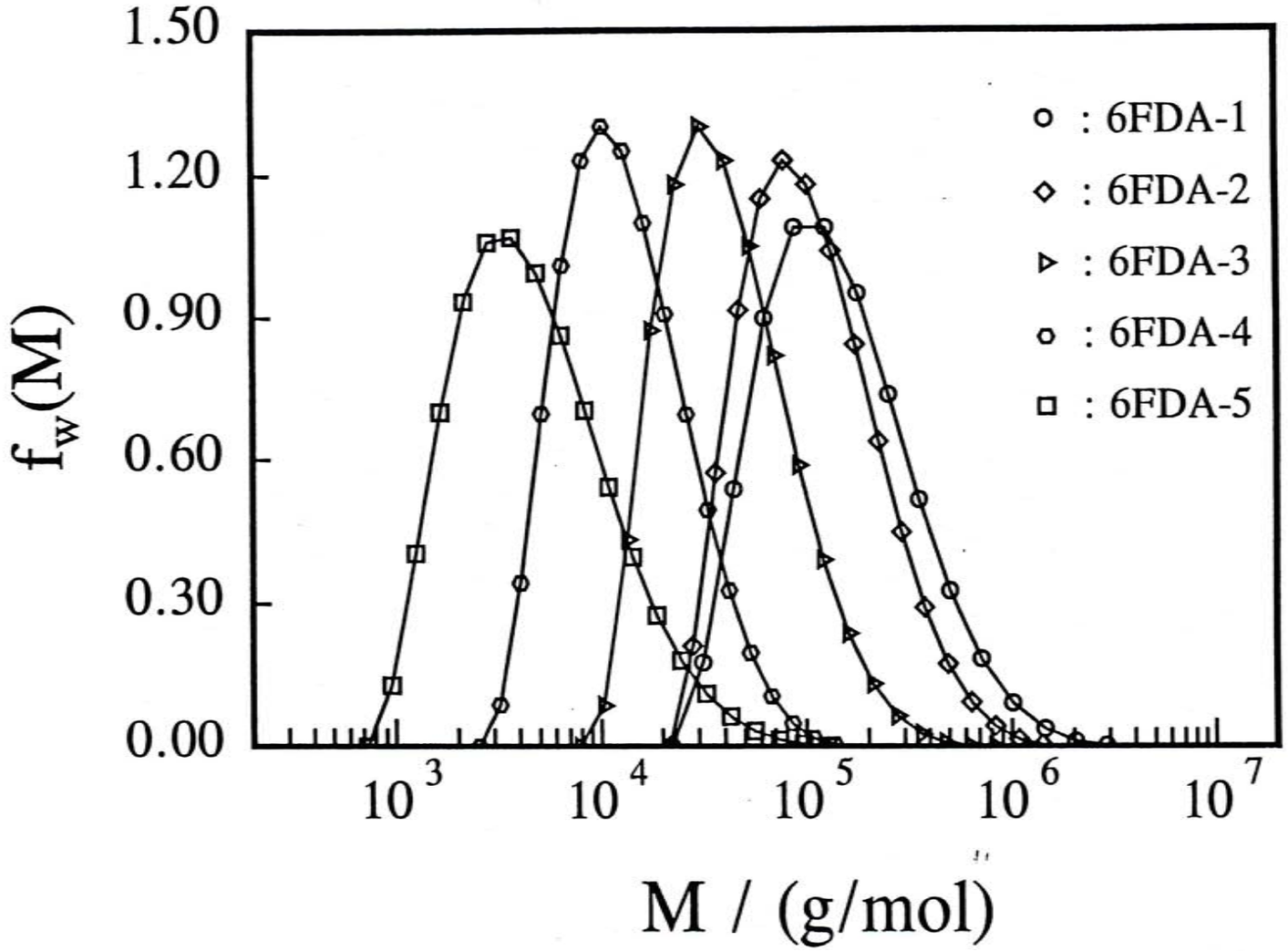


**Figure 4.3.5** Molar mass distributions of five 6FDA-PFMB fractions.

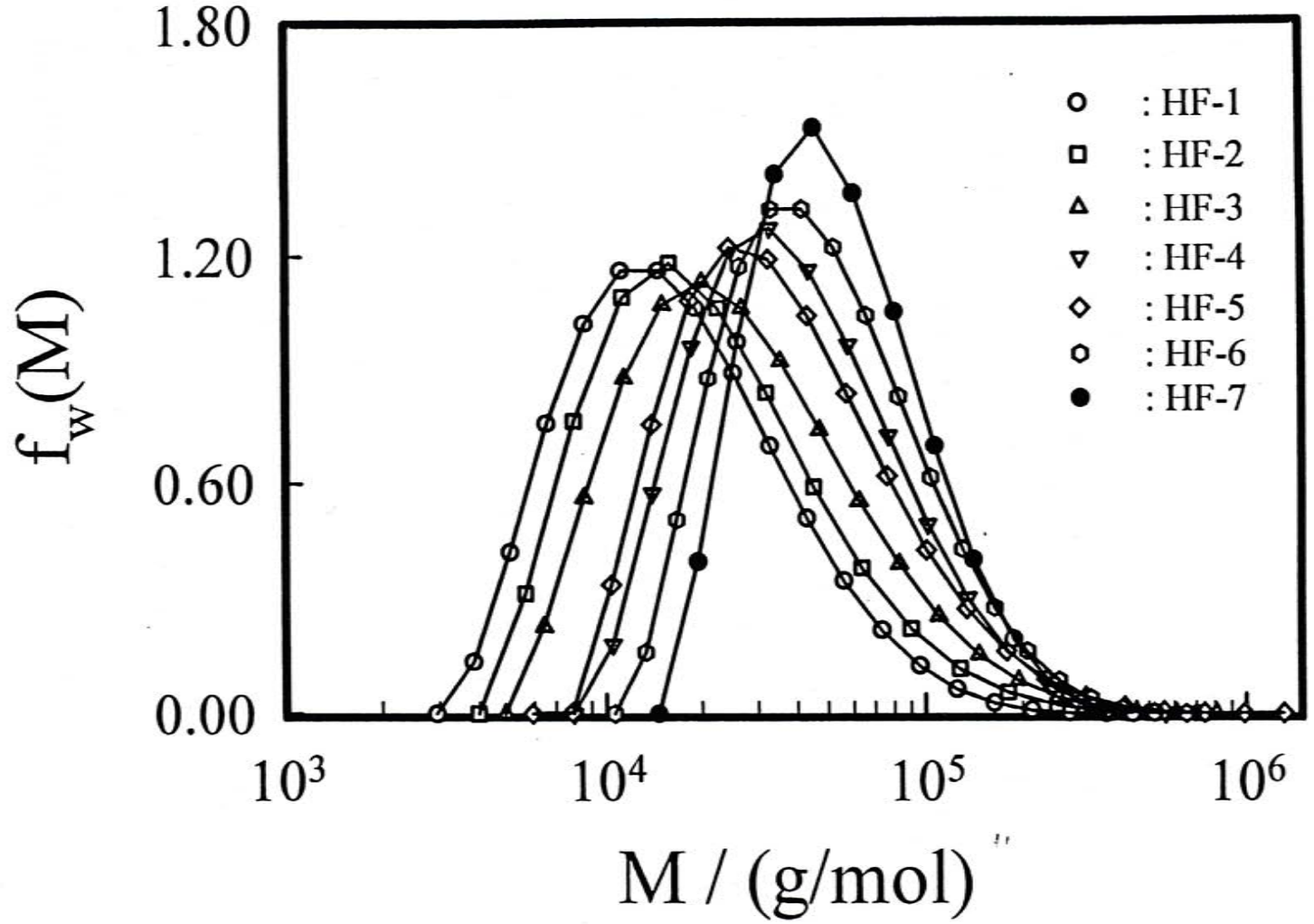


**Figure 4.3.6** Molar mass distributions of seven HFBPDA-PFMB fractions.

the projected length of the monomer unit and n (= $M_w/M_o$) being the average number of the monomers unit of polymer chain. In these case, $\ell_u$ and $M_o$ are, for 6FDA-PFMB: ~ 2.18 nm and 728 g/mol respectively, and for HFBPDA-PFMB: ~ 2.08 nm and 714 g/mol respectively. Strictly speaking, we should use n = $(M_z/M_w)(M_w/M_o)$ since $\langle R_g \rangle$ measured in static LLS is a *z*-averaged parameter. The values of $q$ estimated from the values of $\langle R_g^2 \rangle$ and $M_w$ of 6FDA-PFMB and HFBPDA-PFMB are ~ 3.3 nm and ~ 4.5 nm respectively. In comparison with the value of $q$ ~ 1 nm for typical flexible polymers, such as polystyrene and polymethyl methacrylate in good solvent, the both polyimides chains have a more extended conformation in THF at 30 °C. The extended conformation can be attributed to the rigid segments in the backbone. It is also possible that the extended conformation is related to the excluded volume effect[16]. Eq 2.4.10 shows that when $L/q \rightarrow 0$, $\langle R_g^2 \rangle \rightarrow L^2/12$ and the polymer becomes a rigid rod; on the other hand, when $L/q >> 1$, the polymer chain becomes a coil and $\langle R_g^2 \rangle = \langle h^2 \rangle/6$, where $\langle h^2 \rangle$ (= $2qL$) is the mean square end-to-end distance of the polymer chain. Assuming the both polyimides chains have a coil conformation, the estimate of $q$ from $\langle R_g^2 \rangle$ through $\langle h^2 \rangle$ are ~ 3.3 nm and ~ 4.5 nm for 6FDA-PFMB and HFBPDA-PFMB, respectively, which are very close to the results calculated on the basis of eq 2.4.10, implying that the both polyimides chains have an extended coil conformation.

The coil conformation can be attributed to the rotating joints, such as -O-, -S-, -$CH_2$-, and a single bond between the rigid-rod segments[16,17]. Since the flexibility contributed by -$CH_2$- is normally greater than that by a single bond. Therefore, the coil conformation of the HFBPDA-PFMB chain is more extended which is supported by the higher persistence length and the greater values of the exponents of the

calibrations of HFBDPA-PFMB.

Figures 4.3.7 shows a comparison of the chain dimensions of 6FDA-PFMB and HFBPDA-PFMB with polystyrene in good solvent. The comparisons were calculated by the calibrations $\langle R_g \rangle \sim N$ and $\langle R_h \rangle \sim N$ of the polymers where N is the average number of C-C bonds of the polymer chain. The average number of C-C bonds per monomer unit are 2, 14.2 (2.18 ÷ 0.154) and 13.5 (2.08 ÷ 0.154) for polystyrene, 6FDA-PFMB and HFBPDA-PFMB respectively. The calibrations are, for polystyrene[28], $R_g$ (nm) = 1.13 x $10^{-1}N^{0.620}$ and $R_h$ (nm) = 9.77 x $10^{-2}N^{0.577}$; for 6FDA-PFMB: $R_g$ (nm) = 3.62 x $10^{-1}N^{0.568}$ and $R_h$ (nm) = 2.17 x $10^{-1}N^{0.560}$; for the HFBPDA-PFMB: $R_g$ (nm) = 2.69 x $10^{-1}N^{0.626}$ and $R_h$ (nm) = 1.51 x $10^{-1}N^{0.620}$. The ratios (~ 2) indicate that the coil conformation of the both polyimides is more expanded than that of polystyrene. This expansion is attributed to the excluded volume effect and the chain stiffness. $\langle R_g \rangle_2/\langle R_g \rangle_p$ and $\langle R_h \rangle_2/\langle R_h \rangle_p$ is higher than $\langle R_g \rangle_1/\langle R_g \rangle_p$ and $\langle R_h \rangle_1/\langle R_h \rangle_p$ respectively which indicates that the HFBPDA-PFMB chains are more extended than the 6FDA-PFMB chains. It is noted that $\langle R_g \rangle_1/\langle R_g \rangle_p$ and $\langle R_g \rangle_2/\langle R_g \rangle_p$ are higher than $\langle R_h \rangle_1/\langle R_h \rangle_p$ and $\langle R_h \rangle_2/\langle R_h \rangle_p$ respectively which reveals that both $\langle R_g \rangle_1/\langle R_h \rangle_1$ and $\langle R_g \rangle_2/\langle R_h \rangle_2$ are higher than $\langle R_g \rangle_p/\langle R_h \rangle_p$. This again means that the both polyimides chains are more expanded than polystyrene in good solvent.

## 4.4 Conclusion

A combination of static and dynamic laser light scattering (LLS) studies of 6FDA-PFMB and HFBPDA-PFMB in THF at 30 °C shows that i) the persistence lengths ($q$) of 6FDA-PFMB and HFBPDA-PFMB are ~ 3.3 nm and ~ 4.5 nm respectively and the ratios of $\langle R_g \rangle/\langle R_h \rangle$ are in the range of 1.7-1.9; ii) $\langle R_g \rangle$, $\langle R_h \rangle$

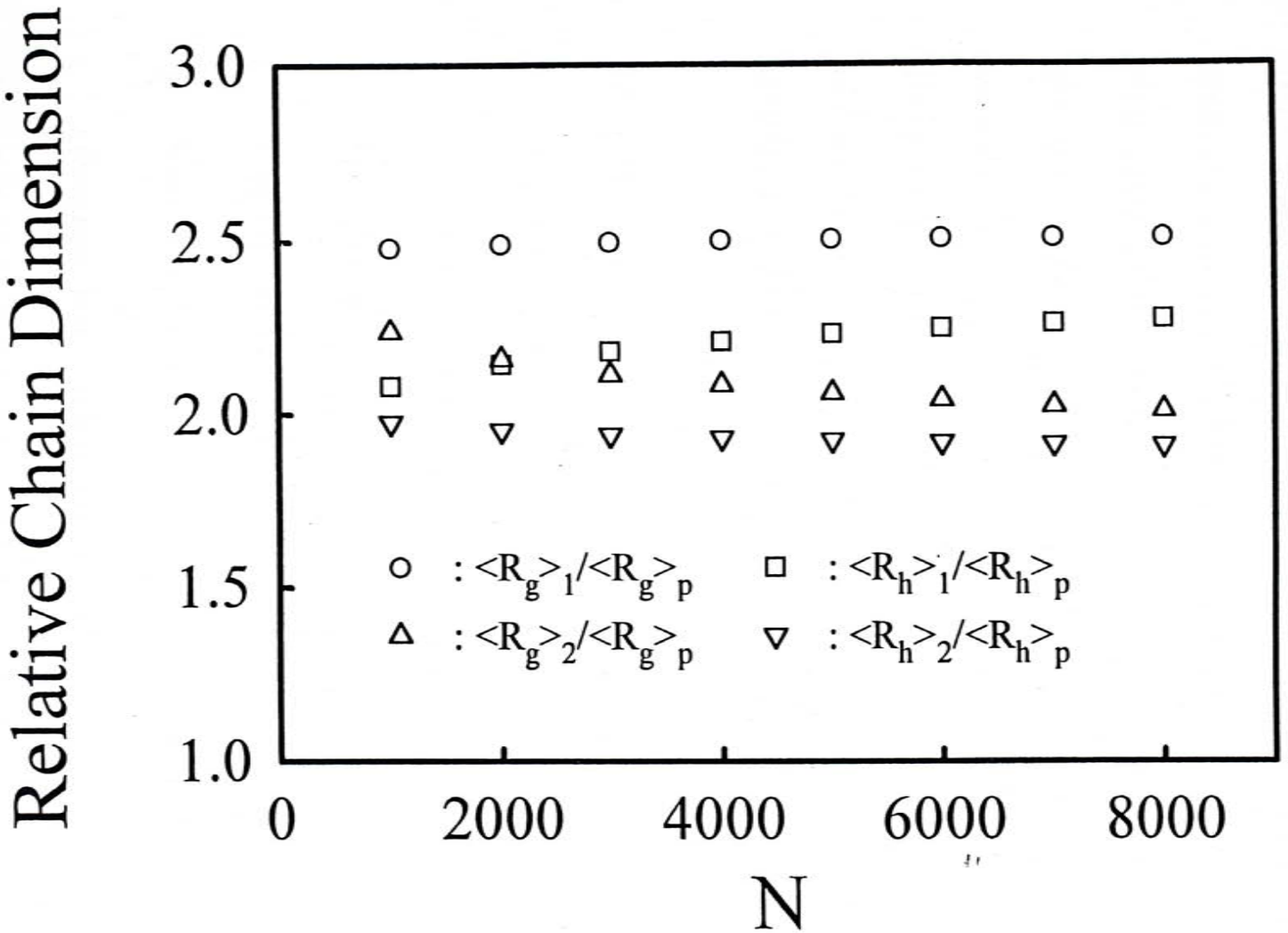


**Figure 4.3.7** Plots of $\langle R_g \rangle_1 / \langle R_g \rangle_p$ vs N (O), $\langle R_h \rangle_1 / \langle R_h \rangle_p$ vs N (□), $\langle R_g \rangle_2 / \langle R_g \rangle_p$ vs N (Δ) and $\langle R_h \rangle_2 / \langle R_h \rangle_p$ vs N (∇) where subscipts 1, 2 and p denote for 6FDA-PFMB, HFBPDA-PFMB and polystyrene respectively.

and D can be scaled to the molar mass as for 6FDA-PFMB: $\langle R_g \rangle$ (nm) = 3.87 x $10^{-2} M_w^{0.568}$, $\langle R_h \rangle$ (nm) = 2.38 x $10^{-2} M_w^{0.560}$ and D ($cm^2/s$) = 2.41 x $10^{-4} M_w^{-0.564}$, for HFBPDA-PFMB: $\langle R_g \rangle$ (nm) = 2.24 x $10^{-2} M_w^{0.626}$, $\langle R_h \rangle$ (nm) = 1.27 x $10^{-2} M_w^{0.621}$ and D ($cm^2$/sec) = 6.16 x $10^{-4}$ x $M^{-0.656}$, respectively; iii) both 6FDA-PFMB and HFBPDA-PFMB chains have an expanded coil conformation; and iv) the HFBPDA-PFMB chains are more extended than the 6FDA-PFMB chains because HFBPDA-PFMB chains contain a less flexible single bond joint instead of a more flexible -$CH_2$- joint in 6FDA-PFMB chains. Using the calibration between D and M, we have successfully converted each translational diffusion coefficient distribution into a corresponding molar mass distribution, which demonstrates that the molar mass distribution of 6FDA-PFMB and HFBPDA-PFMB can be easily characterized in LLS using only one dilute solution measured at one scattering angle.

## 4.5 References


1. Adrova, N. A.; Aleksandrovna, Nina. *Polyimides: a new class of heat-resistant polymers*; Jerusalem, 1969

2. Wilson, D.; Stengenberger, H. D.; Hergenrother P. M. *Polyimides, Chapman and Hall*; New York, 1990

3. Kirby, A. J. *Polyimides: materials, processing and application*; shrewsbury, shropshire: Rapra Technology, Ltd., 1992

4. Cotts, P. M. in *Polyimides: synthesis, characterization, and applications*; Plenum: New York, 1984.

5. Kim, S.; Cotts, P. M.; Wolksen, W. *J. Poly. Sci. part B.* **1992**, *30*, 177

6. Matsuura, T.; Hasuda, Y.; Nishi, S.; Yamada, N. *Macromolecule* **1991**, *24*, 5001

7. Cheng, S. Z. D.; Wu, Z. Q.; Eashoo, M.; Hsu, S. L. C.; Harris, F. W. *Polymer* **1991,** *32*, 1803

8. Feiring, A. E.; Auman, B. C.; Wonchoba, E. R. *Macromolecules* **1993**, *26*, 2779

9. Matsuura, T.; Ishizawa, M.; Hasuda, Y.; Nishi, S. *Macromolecules* **1992**, *25*, 3540

10. Hougham, G.; Tesoro, G.; Shaw, J. *Macromolecules* **1994**, *27*, 3642

11. Hsu, S. L.-C *Ph.D Dissertation*, Department of Polymer Science, The University of Akron, Akron, Ohio, 44325-3909, 1991

12. Lin, S. *Ph.D Dissertation*, Department of Polymer Science, The University of Akron, Akron, Ohio, 44325-3909, 1994

13. Brown, W.; Nicolai, T. in *Dynamic Light Scattering: The method and some application*; W. Brown Eds., Oxford University Press Inc., New York, 1993

14. Wu, C.; Chan, K. K.; Xia, K. Q. *Macromolecules* **1995**, *28*, 1032

15. Burchard, W.; Schmidt, M.; Stockmayer, W. H. *Macromolecules* **1980**, *13*,

1265

16. Magarik, S. Ya. in *Polyamic acids and polyimides: synthesis, transformations, and structure*; Bessonov, M. I. and Zubkov, V. A. Eds.; CRC Press, 1993

17. Pavlova, S. -S. A.; Timofeeva, G. I.; Ronova, I. A. *J. Polym. Sci. Polym. Phys.Ed.* **1980**, *18*, 1175

18. Appelt, B.; Meyerhoff, G. *Macromolecules* **1980**, *13*, 657

# Chapter 5

## Characterization of novel optically active conjugated polyarylenes and poly(aryleneethynylene)s by a combination of Laser Light Scattering and Gel Permeation Chromatography

### 5.1 Introduction

Recently, the investigation of conjugated polymers has attracted much interest because of their useful properties, such as electroluminescence, non-linear optical properties, and high conductivity upon dopping.[1] However, only few studies of optically active conjugated polymers in solution have been reported,[2-4] which might be due to their poor solubility. In the past, the chirality of most optically active conjugated polymers was attributed to their optically active side groups, such as a polyacetylene with optically active alkyl groups.[2] In this study, several novel soluble optically active conjugated polyarylenes and poly(aryleneethynylene)s, which were prepared through a coupling of chiral binaphthyl monomers with various linkers,[5-7] were studied. The chirality was originated from a restricted rotation of the binaphthyl units in their backbone chains. These novel polymers have a high thermal stability. Moreover, they are highly fluorescent and able to emit blue light when irradiated. Recently, it has been shown that polybinaphthol, one of these optically active conjugated polymers, is an excellent polymeric Lewis acid catalysts for the Mukaiyama aldol reaction of benzaldehyde and 1-phenyl-1-(trimethylsilyloxy)-ethylene.[8] The optimization of the synthesis and development of various applications of the novel polymers requires the characterization of their molecular parameters, such as molar mass distribution and chain flexibility.

Gel permeation chromatography (GPC) as a convenient analytical method has been widely used in polymer research and development to determine the molar mass distribution of a given polymer. The calibration of a GPC column normally requires a set of narrowly distributed polymer samples which are rather difficult, if not impossible, to obtain in practice. This is why polystyrene standards are often used if the polymer studied has a similar chain conformation in solution. However, in this study, the chain conformations of polyarylenes and poly(aryleneethnylene)s are expected to be quite different from that of polystyrene. Therefore, we have to adopt a recently developed method of combining the LLS and GPC results of only one sample to calibrate the GPC columns which has been discussed in chapter 2. Eight different polyarylenes and poly(aryleneethynylene) samples were investigated and their molecular structures are as follows:

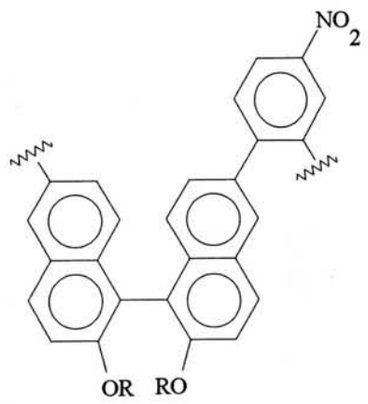


(1) (*R*)-Hu-1-129
(2) *Rac*-Hu-1-130
R=$C_6H_{13}$

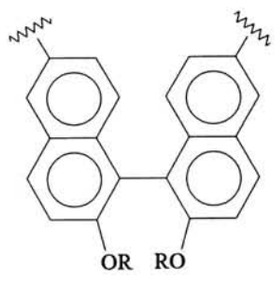


(3) (*R*)-Hu-1-211
(4) *Rac*-Hu-1-209
R=Ac

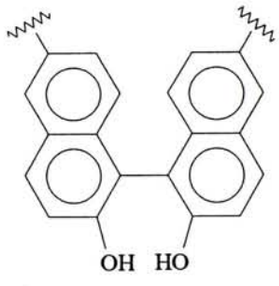


(5) (*R*)-Hu-1-215

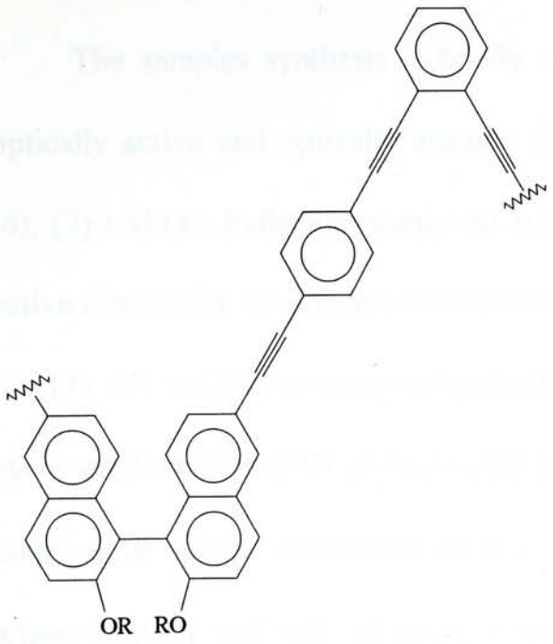


(6) *Rac*-Ma-1-159
R=$C_{18}H_{37}$

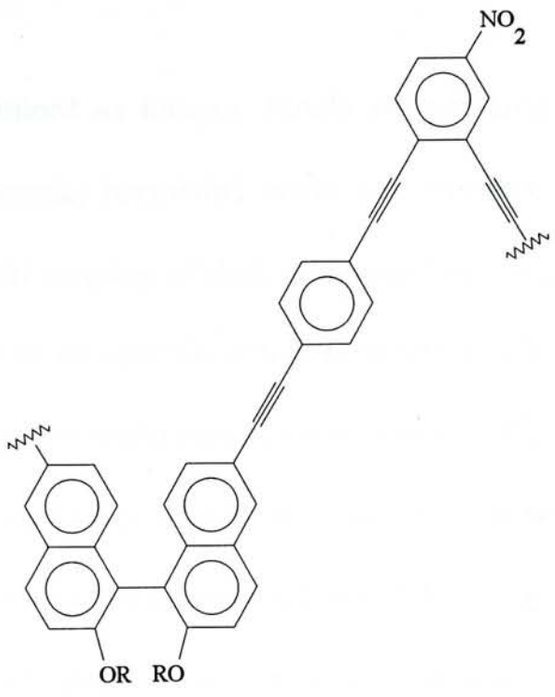


(7) *Rac*-Ma-1-157
R=$C_{18}H_{37}$

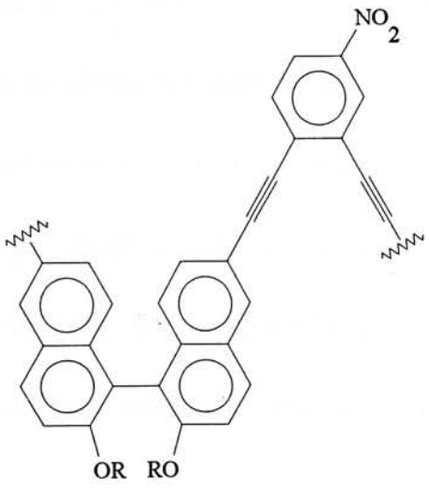


(8) (*R*)-Ma-1-148
R=$C_{18}H_{37}$

where (*R*) and *Rac* stand for the optically active and inactive polymers respectively. Polyarylenes and poly(aryleneethynylene)s are soluble in various organic solvents such as THF and chloroform in spite of their rigid backbone chain structure. It is due to the reduction of the π-π stacking by the nonplanarity of the binaphthyl groups.

## 5.2 Sample preparation

The samples synthesis is briefly outlined as follows. Firstly we prepared the optically active and optically inactive (racemic) binaphthyl monomers. For (1), (2), (6), (7) and (8), Palladium-catalyzed Suzuki coupling of their corresponding optically active monomers of different linkers leads to an optically active conjugated polymer. For (3), (4) and (5), coupling of optically active monomers in the presence of bis(1,5-cyclooctadiene)nickel(0) gives an optically active polymers. With the same methods, coupling of racemic monomers leads to an optically inactive polymer. The chirality is arisen from the well-ordered arrangement of binaphthyl groups in the backbone which is achieved by the regioselectivity of the catalysts and the restricted rotation of the binaphthyl groups. The propagation of the backbone of optically active polymers is like a coil. The sample synthesis has been detailed before.[9, 10, 11] Analytical grade THF dried by sodium immediately prior to the sample preparation was used as solvent for all the polymers except (*R*)-Hu-1-215 for which 1 M NaOH was used as solvent because it is insoluble in THF. The solution concentration was in the range $4 \times 10^{-4}$ - $3 \times 10^{-3}$ g/mL. All the polymer solutions were clarified by 0.5μm PTFE filters at room temperature.

## 5.3 Results and Discussion

Figure 5.3.1 shows the concentration dependence of $[KC/R_{vv}(q)]_{q\to 0}$ respectively for *Rac*-Hu-1-130 and (*R*)-Hu-1-211. According to eq A.1.29, $M_w$, $\langle R_g \rangle$ and $A_2$ can be obtained from the extrapolation of $[KC/R_{vv}(q)]_{c\to 0,q\to 0}$, $[KC/R_{vv}(q)]_{c\to 0}$ versus $q^2$ and $[KC/R_{vv}(q)]_{q\to 0}$ versus C, respectively. The LLS results are summarized in Table 5.3.1. In this study, $\langle R_g \rangle$ is so small that $[KC/R_{vv}(q)]$ has nearly no angular

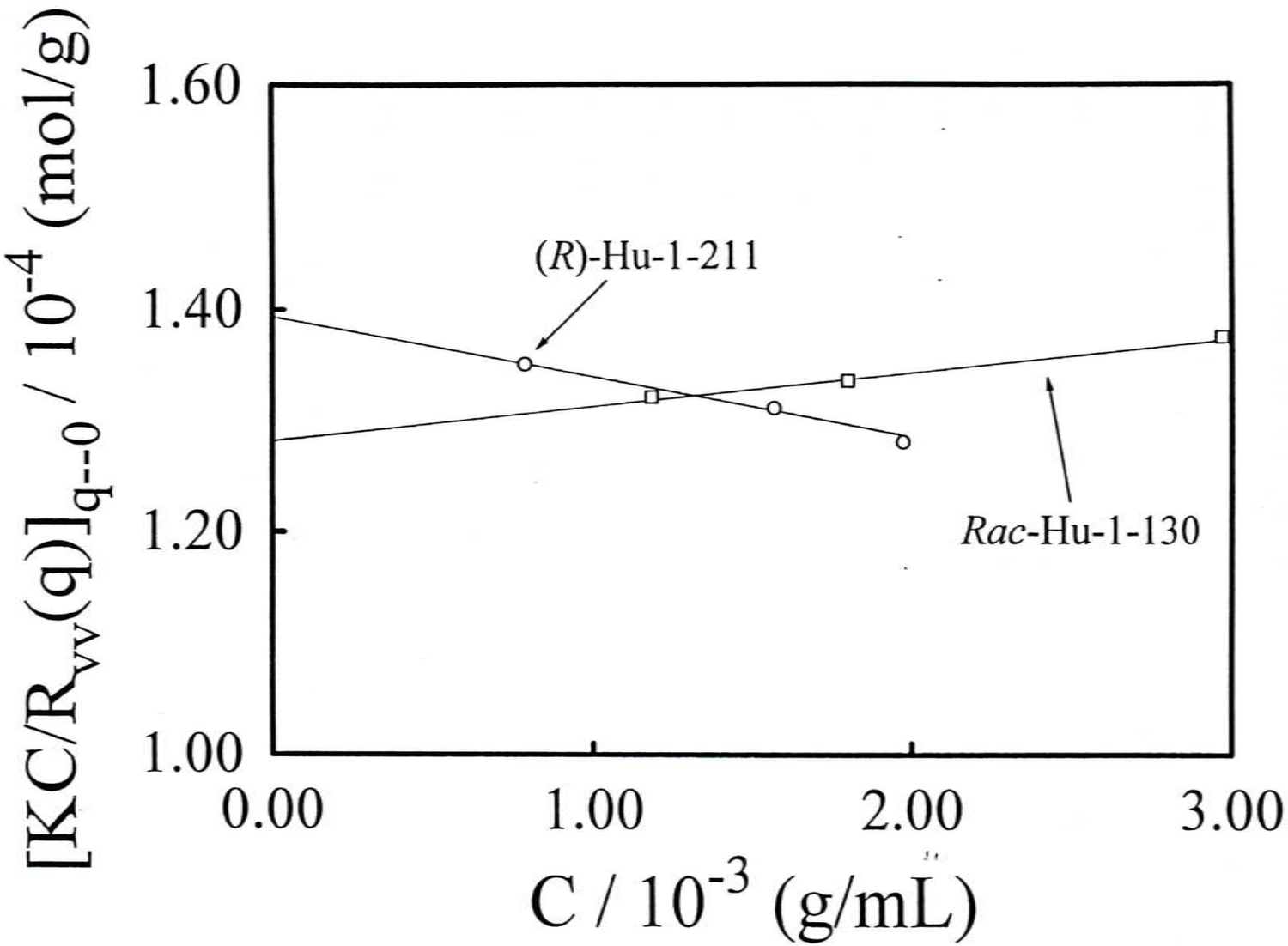


**Figure 5.3.1** Concentration dependence of $[KC/R_{vv}(\theta)]_{q\to 0}$ of (*Rac*)-Hu-1-130 and (*R*)-Hu-1-211 in THF at T = 25°C.

**Table 5.3.1** Summary of Static and Dynamic Laser Light-Scattering results of polyarylenes and poly(aryleneethynylene)s in THF at 25°C

| Sample | $M_w$ (g/mol) | $10^3A_2$ (mol·cm$^3$/g$^2$) | $10^8$<D> (cm$^2$/s) | <$R_h$> (nm) | dn/dC (mL/g) | $M_{w,SEC}$ (g/mol) |
|---|---|---|---|---|---|---|
| (*R*)-Hu-1-129 | 12200 | ~ 0 | 178 | 2.59 | 0.250 | 10100 |
| *Rac*-Hu-1-130 | 7780 | 1.40 | 232 | 1.98 | 0.250 | 6300 |
| (*R*)-Hu-1-211 | 7130 | -2.86 | 202 | 2.28 | 0.291 | 6400 |
| *Rac*-Hu-1-209 | 5930 | -6.27 | 205 | 2.24 | 0.291 | 7400 |
| *Rac*-Ma-1-159 | 13800 | -6.24 | 168 | 2.74 | 0.255 | 11600 |
| *Rac*-Ma-1-157 | 12400 | 2.66 | 142 | 3.24 | 0.267 | 10500 |
| (*R*)-Ma-1-148 | 22000 | 5.15 | 210 | 2.19 | 0.215 | 7200 |

The relative errors: $M_w$, ± 5 %; $A_2$, ± 20 %; <D> and <$R_h$>, ± 5 %; dn/dC, ± 0.002

dependence and no values of $<R_g>$ were obtained. The positive and negative values of $A_2$ respectively indicate that THF is a good solvent for (*Rac*)-Hu-1-130 and *Rac*-Ma-1-157, (*R*)-Ma-1-148 and (*R*)-Hu-1-215 and a poor solvent for (*R*)-Hu-1-211 and *Rac*-Hu-1-209 and *Rac*-Ma-1-159. It is clear that introducing the $-NO_2$ groups can promote the solubility in THF.

Figure 5.3.2 shows a typical intensity-intensity time correlation function of (*R*)-Hu-1-129 in THF at 25 °C, where the insert shows a corresponding line width distribution $G(\Gamma)$ calculated on the basis of eq A.2.19 by using the CONTIN program. It is surprising to find that $G(\Gamma)$ is narrow for all the polymers studied and the relative width $\mu_2/<\Gamma>^2$ is in the range of 0.2 ~ 0.3, where $\mu_2 = \int_0^\infty G(\Gamma)(\Gamma - <\Gamma>)^2 d\Gamma$ and $<\Gamma> = \int_0^\infty G(\Gamma)\Gamma d\Gamma$. The line width $\Gamma$ can be further converted to the translational diffusion coefficient D on the basis of eq A.2.20. In the case of $C \sim 10^{-4}$ and $\theta < 30°$, $(1 + k_d C)(1 + f<R_g^2>_z q^2) \sim 1$ so that $\Gamma/q^2 \approx D$. $G(\Gamma)$ can be directly converted into a translational diffusion coefficient distribution G(D).

Figure 5.3.3 shows translational diffusion coefficient distributions G(D) of polyarylenes and poly(aryleneethnylene)s in THF at 25°C. G(D) can be further related to a hydrodynamic radius distribution $f(R_h)$ using the Stokes-Einstein equation: $D \equiv kT/(6\pi\eta R_h)$, where k, T, and $\eta$, are the Boltzmann constant, the absolute temperature, and solvent viscosity, respectively. All dynamic LLS results are also summarized in Table 5.3.1, where $<D> = [\int_0^\infty G(D)D\, dD]$ and $<R_h> = k_B T/6\pi\eta<D>$. The small values of $<R_h>$ indicate that all the polymer chains are short, which are consistent with their low molar masses.

(*R*)-Hu-1-215 is insoluble in THF, but is partially soluble in 1M NaOH aqueous

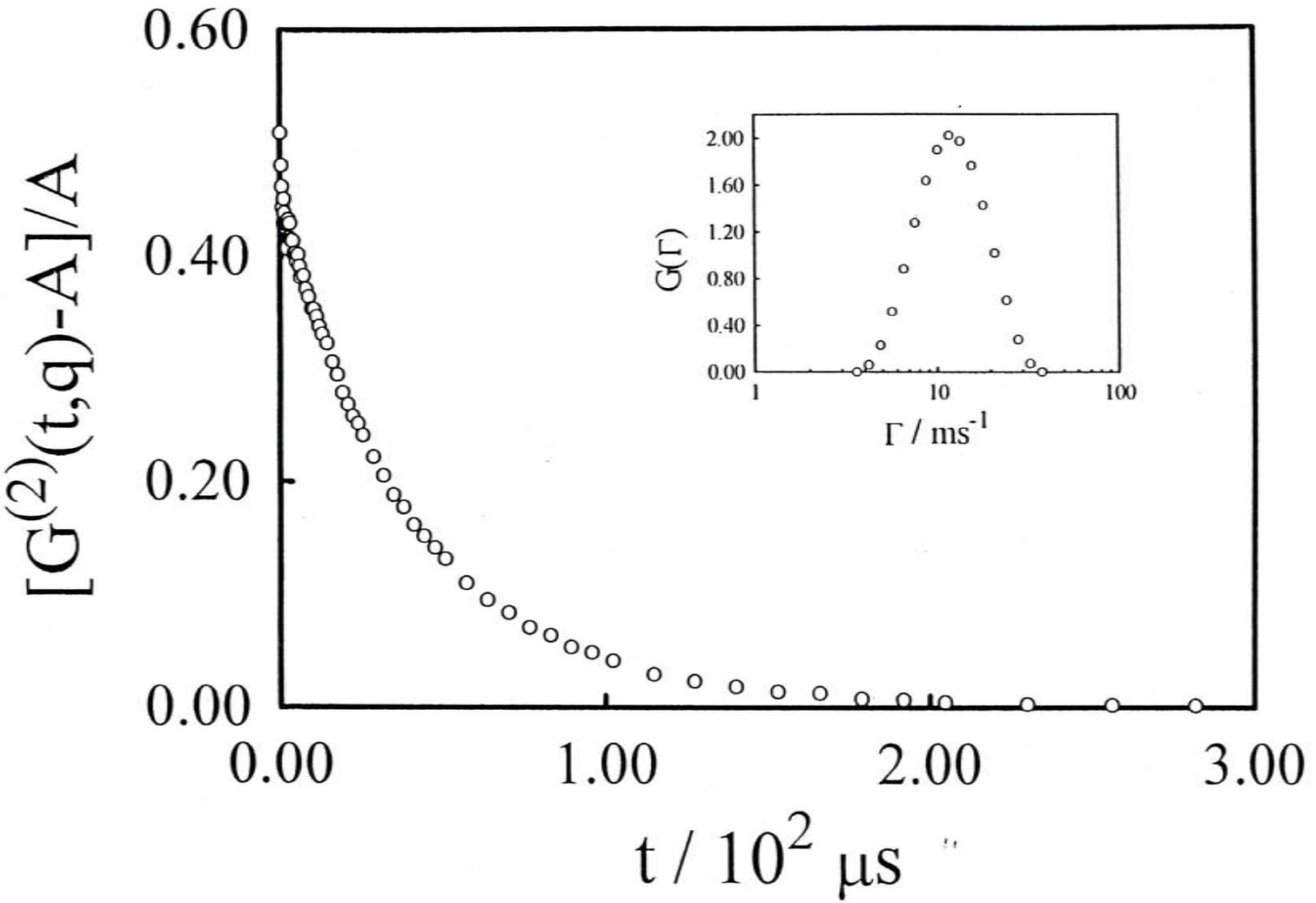


**Figure 5.3.2** Typical measured intensity-intensity time correlation function of (*R*)-Hu-1-129 in THF at $\theta = 30^{\circ}$ and $T = 25^{\circ}C$, where the insert shows a corresponding line-width distribution $G(\Gamma)$ calculated from $G^{(2)}(t,q)$ on the basis of eqs 2.2.19 and 2.2.21.

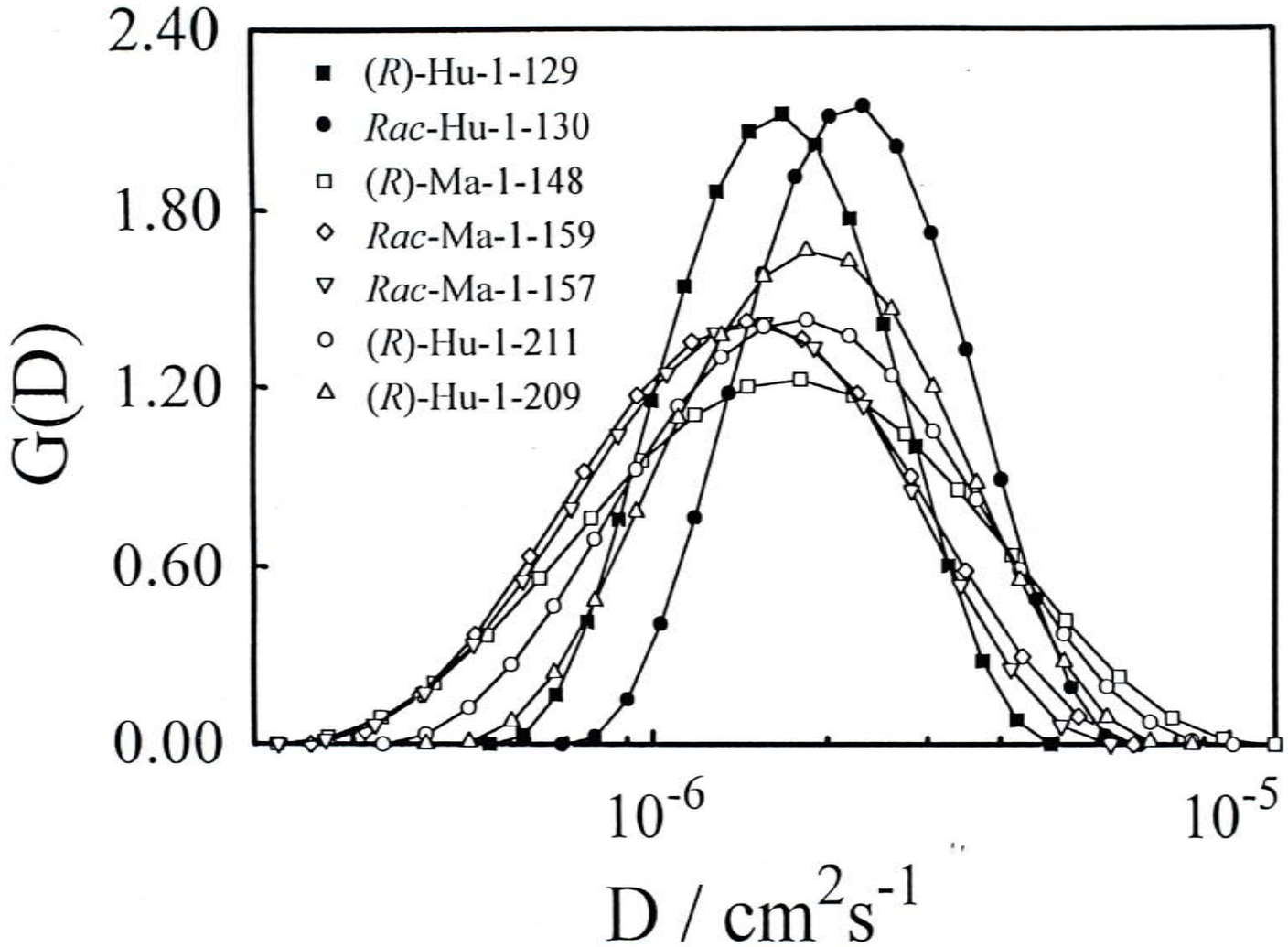


**Figure 5.3.3** Translational diffusion coefficient distributions of seven polyarylene and poly(aryleneethynylene) samples in THF at 25°C.

solution, evidenced by a bimodel hydrodynamic radius distribution shown in Figure 5.3.4. The first peak located in the range of 1-9 nm represents individual polymer chains and the second peak located at ~100 nm could be attributed to either the aggregation of individual polymer chains or possible electrostatic interaction between the hydroxyl groups ionized in the strong base solution. However, we found that adding 0.1M NaCl into the solution to increase the ionic strength of the solution has no effect on $f(R_h)$, which indirectly indicates that the second peak is related to the aggregation. It is interesting to note that the only difference between (*R*)-Hu-1-211 and (*R*)-Hu-1-215 is that the -OAc groups have been replaced by the -OH groups.

For comparison, the values of $M_w$ from GPC in which polystyrene standards were used to calibrate the columns are also listed in Table 5.3.1. Except in the case of (*R*)-Ma-1-148, LLS gives a larger $M_w$ than SEC, indicating that using polystyrene to calibrate the GPC columns is improper because the polyarylene and poly(aryleneethynylene) chains are more rigid. The LLS study of other poly(aryleneethynylene)s also showed a similar result.[12] Considering the results of (*R*)-Hu-1-211 and *Rac*-Hu-1-209, we think that the LLS results are more reasonable because the variation of $M_w$, $A_2$ and $R_h$ is consistent; namely, $A_2$ increases and $R_h$ decreases as $M_w$ decreases. Ideally, we should use a set of samples with different molar masses, but the same chemical structure, to calibrate the GPC columns. However, in this study, we failed to obtain different molar masses for each sample since the synthesis is rather difficult.

In order to obtain a proper calibration of the GPC columns from only one polymer sample, we used a method of combining the off-line LLS and GPC results which has been discussed in chapter 2. This method not only calibrates the GPC

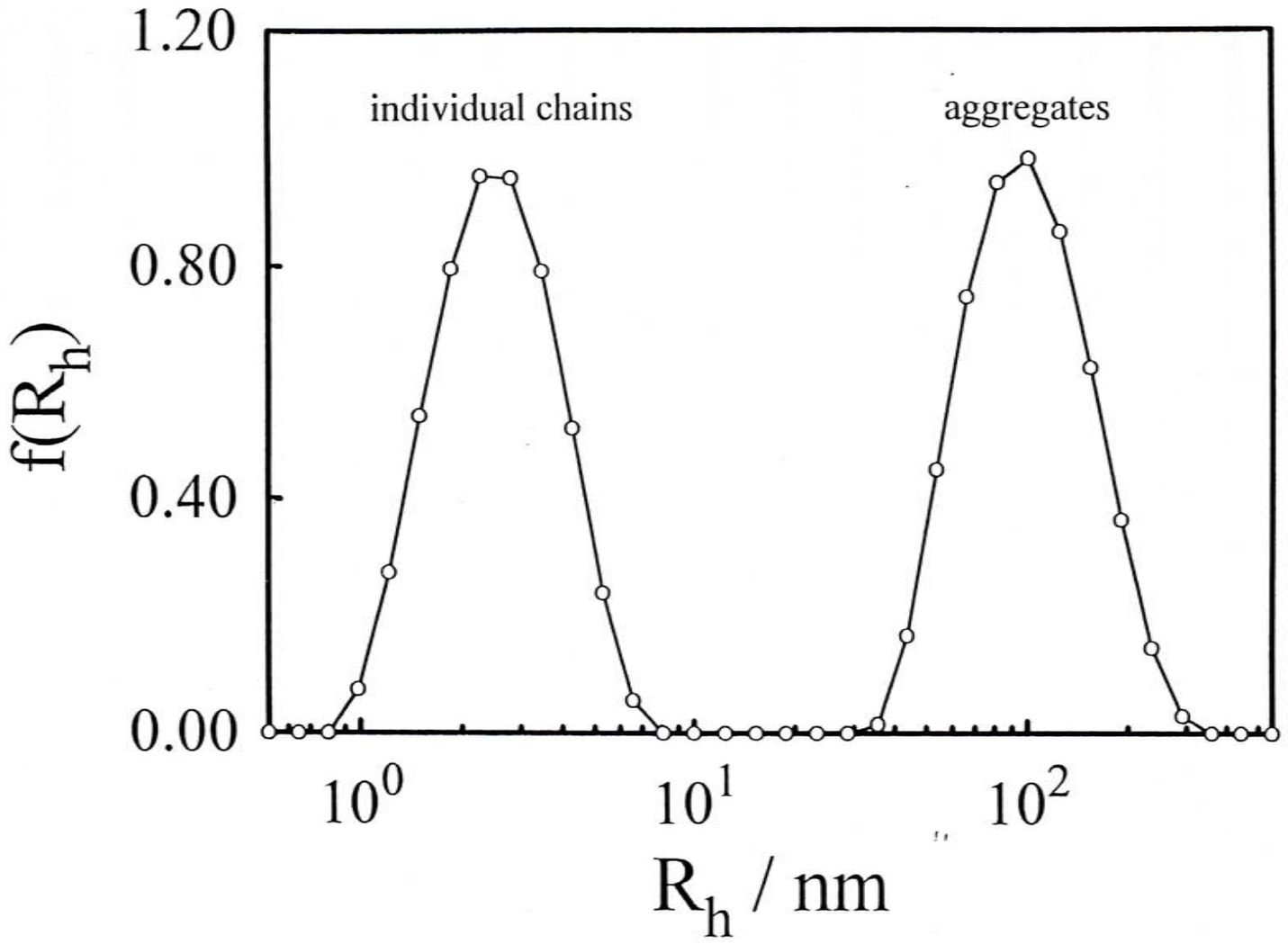


**Figure 5.3.4** Hydrodynamic radius distribution of (*R*)-Hu-1-215 in THF at 25°C.

column, but also obtain the calibrations: $V=A+B\log(M)$ and $D=k_D M^{-\alpha_D}$.

Table 5.3.2 summarizes the values of A, B, $k_D$ and $\alpha_D$. The fact that $\alpha_D = 1$ indicates that the polymer chains have a rigid conformation. This is expected because the conjugated backbone chains with the bulk binaphthyl groups are so short (10 ~ 20 monomer units) that they are not flexible. Moreover, it is worth noting that the calibration parameters are similar, which can be attributed to a similar rod-like structure of these conjugated polymers.

Once having A, B, $k_D$ and $\alpha_D$, we were ready to convert either G(D) or C(V) into a corresponding molar mass distributions $F_w(M)$. Figures 5.5 and 5.6 respectively show such calculated molar mass distributions from G(D) and C(V), respectively. It should be stated that the difference in the low molar mass tail of the distributions presented in Figure 5.5 and 5.6 is due to the fact that the LLS detector is not able to "see" the lower molar mass portion because the scattered light intensity is proportional to $M^2$. The polydispersity index ($M_w/M_n$) calculated from the $F_w(M)$s in Figures 5.5 and 5.6 are also summarized in Table 5.3.2. Both the values of $M_w$ and $M_w/M_n$ calculated from G(D) and C(V) agree satisfactorily well with each other.

## 5.4 Conclusions

It is clear that using polystyrene to calibrate the GPC columns for the characterization of the molar mass distribution of polyarylene or poly(aryleneethynylene) can lead to an improper $M_w$. A combination of laser light scattering and gel permeation chromatography has established the calibrations of $V = A + B\log(M)$ and $D = k_D M^{-\alpha_D}$ for polyarylene and poly(aryleneethynylene) in THF at 25°C. Using these calibrations, we were able to estimate the molar mass distributions

**Table 5.3.2.** Summary of the calibration constants and the parameters of the molar mass distributions

| | | | | | From G(D) | | From C(V) | |
|---|---|---|---|---|---|---|---|---|
| Sample | A | B | $10^2 k_D$ ($cm^3$) | $\alpha_D$ ($cm^3$) | $M_w$ ($cm^2/s$) | $M_w/M_n$ | $M_w$ (g/mol) | $M_w/M_n$ (g/mol) |
| (*R*)-Hu-1-129 | 45.8 | -2.61 | 2.17 | 1 | 12200 | 1.16 | 12100 | 1.16 |
| *Rac*-Hu-1-130 | 42.2 | -2.28 | 1.82 | 1 | 7780 | 1.15 | 7760 | 1.15 |
| (*R*)-Hu-1-211 | 42.6 | -2.34 | 1.44 | 1 | 7130 | 1.14 | 7130 | 1.14 |
| *Rac*-Hu-1-209 | 41.7 | -2.31 | 1.22 | 1 | 5930 | 1.26 | 5890 | 1.25 |
| *Rac*-Ma-1-159 | 36.7 | -1.66 | 2.32 | 1 | 13800 | 1.35 | 13600 | 1.35 |
| *Rac*-Ma-1-157 | 37.2 | -1.72 | 1.77 | 1 | 12400 | 1.31 | 12200 | 1.31 |
| (*R*)-Ma-1-148 | 32.5 | -1.11 | 4.63 | 1 | 22000 | 1.50 | 21600 | 1.49 |

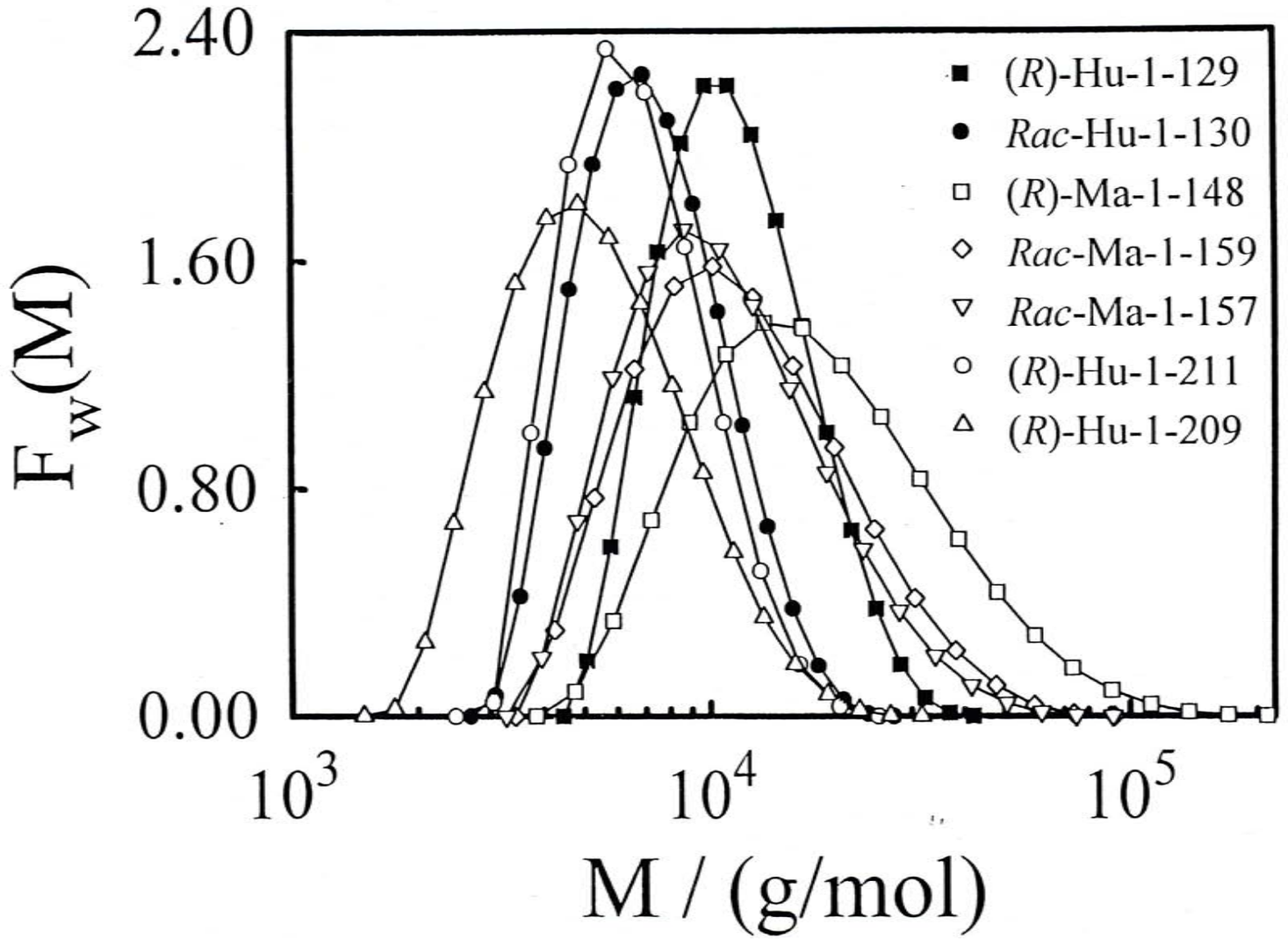


**Figure 5.3.5** Differential weight distributions ($F_w(M)$), calculated from the G(D)s from LLS shown in Figure 3, of seven polyarylene and poly(aryleneethynylene) samples.

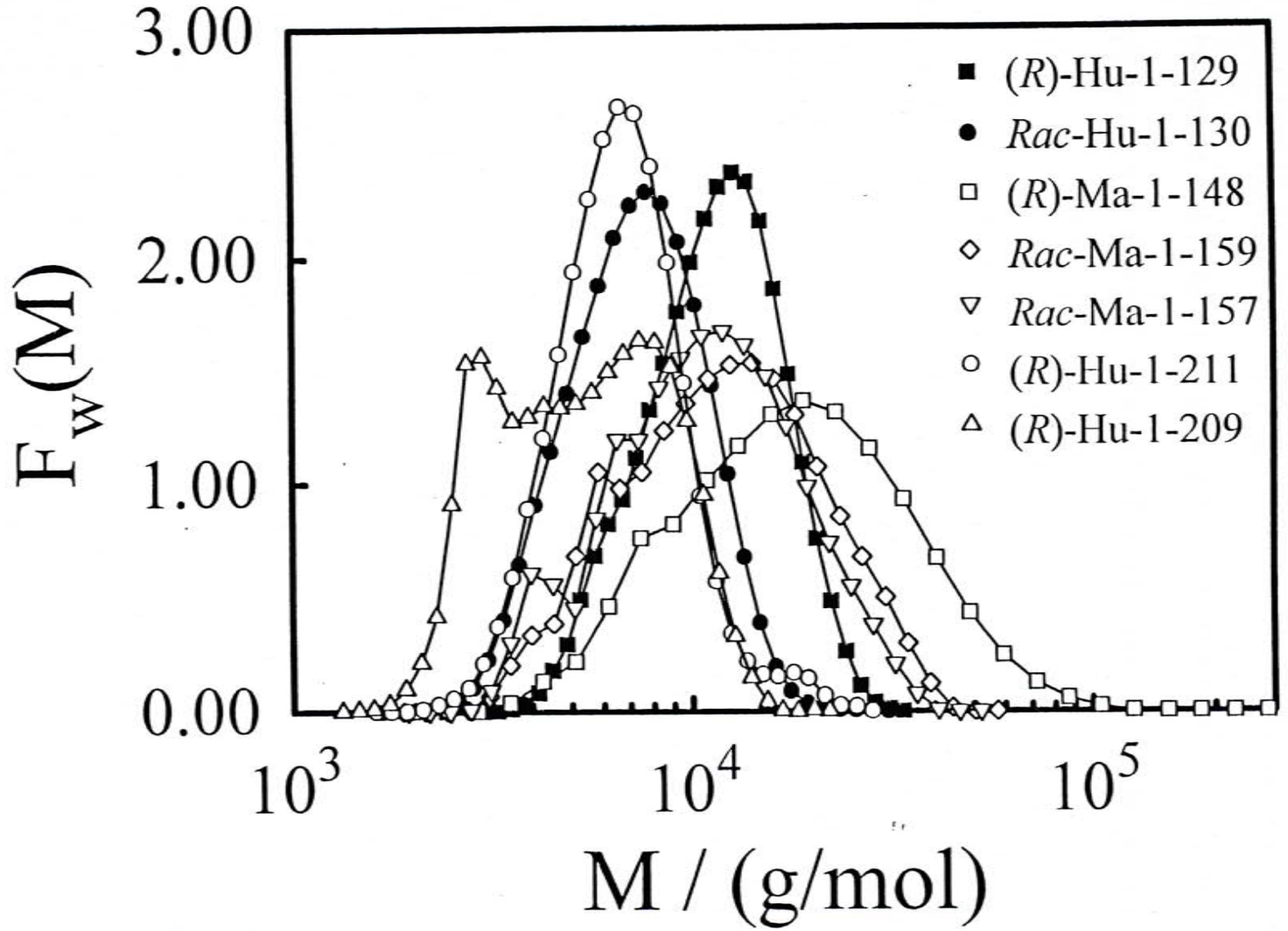


**Figure 5.3.6** Differential weight distributions ($F_w(M)$), calculated from the C(V)s from GPC, of seven polyarylene and poly(aryleneethynylene) samples.

of polymers. Our results reveal that polyarylene and poly(aryleneethynylene) have a rigid chain conformation in THF. Introducing the $-NO_2$ groups into polyarylene and poly(aryleneethynylene) increases its solubility in THF at 25°C. The calibrations of $D = k_D M^{-\alpha_D}$ established in this study are independent of a particular light scattering instrument and ready to be used in future to characterize similar polyarylene and poly(aryleneethynylene) as long as THF is used as solvent and temperature is 25°C.

## 5.4 References


1. Kiess, H. G., Ed. *Conjugated Conducting Polymers*; Springer-Verlag: New York, 1992.
2. Moore, J. S.; Gorman, C. B.; Grubbs, R. H. *J. Am. Chem. Soc.* **1991**, *113*, 1704.
3. Kotkar, D.; Joshi, V.; Ghosh, P. *J. Chem. Soc., Chem. Commun.* **1998**, 917.
4. Lemaire, M.; Delabouglise, D.; Garreau, R.; Guy, A.; Roncali, J. *J.Chem. Soc., Chem. Commun.* **1998**, 658.
5. Hu, Q. S.; Vitharana, D.; Liu, G. Y.; Jain, V.; Wagaman, M. W.; Zhang, L.; Lee, T. R.; Pu, L. *Macromolecules* **1996**, *29*, 1082.
6. Hu, Q. S.; Vitharana, D.; Liu, G. Y.; Jain, V.; Pu, L. *Macromolecules* **1996**, *29*, 5075.
7. Ma, L.; Hu, Q. S.; Musick, K. Y.; Vitharana, D.; Wu, C.; Kwan, C. M. S.; Pu, L. *Macromolecules* **1996**, *29*, 5083.
8. Hu, Q. S.; Vitharana, D.; Zheng, X. F.; Wu, C.; Kwan, C. M. S.; Pu, L. *J. Org. Chem.* **1996**, *61*, 8370.
9. Ma, L.; Hu, Q. S.; Vitharana, D.; Wu, C.; Kwan, C. M. S.; Pu, L. *Macromelcules* **1997**, *30*, 204.
10. Hu, Q. S.; Zheng, X. F.; Pu, L. *J. Org. Chem.* **1996**, *61*, 8370.
11. Hu, Q. S.; Vitharana, D.; Zheng, X. F.; Wu, C.; Kwan, C. M. S.; Pu, L. *J. Org. Chem.* **1996**, *61*, 8370.
12. Yamamoto, T.; Takagi, M.; Kizu, K.; Maruyama, T.; Kubota, K.; Kanbara, H.; Kurihara, T.; Kaino, T. *J. Chem. Soc., Chem. Commun.* **1993**, 797.

# Appendix

## A.1 Static laser light scattering (Static LLS)[1-3]

The electric field of a light wave acting on a particle causes it a induced dipole that oscillates with the same frequency as the incident light. The oscillating dipole produces a secondary oscillating electric field which radiates a light wave. This phenomena is so-called scattering.

**A.1.1 Scattering from a small particle:** If we assume the single particle is optically isotropic with polarizability $\alpha$, and the particle is in vacuum and is much smaller than the wavelength $\lambda_o$ of incident light ($<<\lambda_o/20$). Then intensity of the scattered light is found to be

$$I_s = \frac{16\pi^4\alpha^2}{r^2\lambda_o^4} I_o \qquad \text{(A.1.1)}$$

where $I_o$ and r are the intensity of the incident light and distance from the particle to the detector respectively. In our discussion, both incident light and scattered light are vertically polarized. A variable, $R_{vv}$, is more commonly used and is defined as

$$R_{vv} = \frac{I_s r^2}{I_o} = \frac{16\pi^4\alpha^2}{\lambda_o^4} \qquad \text{(A.1.2)}$$

where the first subscript 'v' means the incident light is vertically polarized and the second subscript 'v' means the scattered light is also vertically polarized. It is called the Rayleigh ratio because it is defined by Rayleigh. $R_{vv}$ is a constant for a given particle in the same experimental condition.

**A.1.2 Scattering from a large particle:** If the size of a particle is comparable to the wavelength of the incident light ($\geq\lambda_0/20$), the particle can be treated to contain n

scattering points which have the same polarizability $\alpha_o$ ($\alpha = n\alpha_o$) and are much smaller than $\lambda_o$. Then the electric field of the scattered light at the detector is the vector sum of that of individual scattering points as shown in Figure A.1.1. They arrive at the detector with different phases and there always exists an destructive interference except the detector is placed at zero angle. The Rayleigh ratio for the whole particle is

$$R_{vv} = \frac{16\pi^4\alpha_o^2}{\lambda_o^4}\sum_{i=1}^{n}\sum_{j=1}^{n}\cos(\varphi_i - \varphi_j) \qquad (A.1.3)$$

where $\varphi_i$ and $\varphi_j$ are the phase difference of the light wave scattered by ith and jth scattering points with respect to some reference wave. If the particle is very small, $\varphi_i$ and $\varphi_j$ are the same so that eqn. (A.1.3) is reduced to eqn. (A.1.2). According to Figure A.1.1, the path difference of light scattered by two scattering points is

$$\Delta_{ij} = \Delta_j - \Delta_i = (a + \mathbf{k}_p \cdot \mathbf{r}_{ij} + b - \mathbf{k}_s \cdot \mathbf{r}_{ij}) - (a + b) = \mathbf{k} \cdot \mathbf{r}_{ij} \qquad (A.1.4)$$

where $\mathbf{k}_p$ and $\mathbf{k}_s$ are unit vectors along transmitted beam and along scattered beam respectively. $\mathbf{r}ij$ is the position vector from point i to point j and the vector $\mathbf{k} \equiv \mathbf{k}_s - \mathbf{k}_p$ and $|\mathbf{k}| = k = 2\sin(\theta/2)$. The phase difference of the two scattered beams is related to $\Delta_{ij}$ as

$$\varphi_i - \varphi_j = 2\pi\Delta_{ij}/\lambda_o \qquad (A.1.5)$$

Combining eqs. (A.1.3 ~ A.1.5) and averaging $\cos(\varphi_i - \varphi_j)$ for all orientations of the position vector $\mathbf{r}_{ij}$ with respect to the vector $\mathbf{k}$ due to the fact that the orientation of the particle changes randomly with time, we obtain

$$R_{vv} = \frac{16\pi^4\alpha_o^2}{\lambda_o^4}\sum_{i=1}^{n}\sum_{j=1}^{n}\frac{\sin qr_{ij}}{qr_{ij}} \qquad (A.1.6)$$

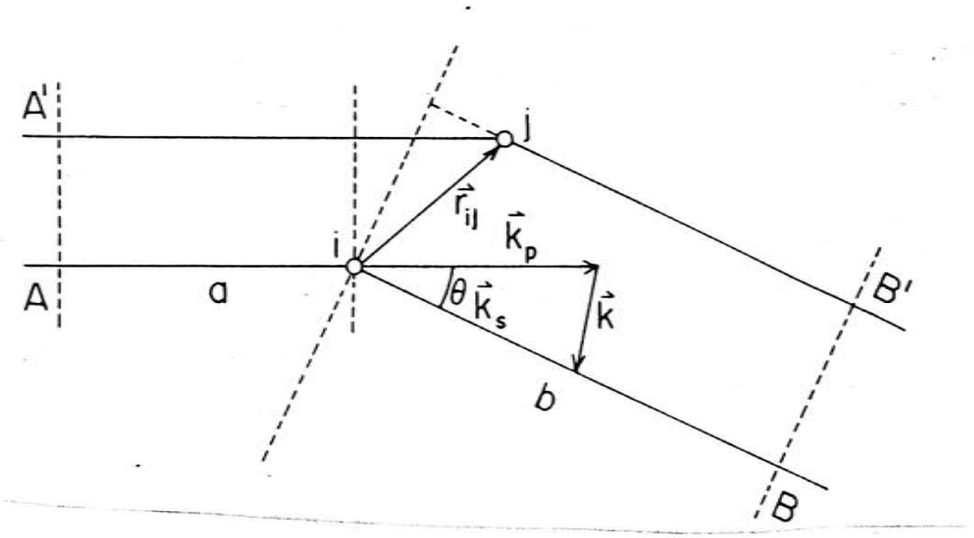


**Figure A.1.1** The path difference of light scattered by two elements

where q is the scattering vector ($4\pi\sin(\theta/2)/\lambda$). It is obvious that $R_{vv}$ is a function of $\theta$ and it becomes a constant ($R_0$: $16\pi^4\alpha^2/\lambda_o^4$) for all particles of the same polarizability irrespective of their size near to zero angle. Therefore, a new function $P(\theta)$, namely particle scattering factor, is defined as

$$P(\theta) = \frac{R_{vv}}{R_0} = \frac{1}{n^2}\sum_{i=1}^{n}\sum_{j=1}^{n}\frac{\sin qr_{ij}}{qr_{ij}} \qquad (A.1.7)$$

eqn. (A.1.7) can be expanded into a Taylor series ($\sin x = x - x^3/6 + \ldots$) and we only keep the first two terms in the expansion owing to small value of $qr_{ij}$, the expression is then changed to

$$P(\theta) = -\frac{q^2}{6n^2}\sum_{i=1}^{n}\sum_{j=1}^{n} r_{ij}^2 \qquad (A.1.8)$$

As $r_{ij}$ is related to the radius of gyration in the following expression

$$\sum_{i=1}^{n}\sum_{j=1}^{n} r_{ij}^2 = 2n^2R_g^2 \qquad (A.1.9)$$

Combining eqs. (A.1.8) and (A.1.9) yields

$$P(\theta) = -\frac{q^2R_g^2}{3} \qquad (A.1.10)$$

If $P(\theta)$ is measured at different q, Rg can be easily obtained. It should be noted that the size of particles measured by static laser light scattering is an absolute method that requires no calibrations. We will see that the size of particles can also be found by dynamic laser light scattering without calibration.

**A.1.3 Scattering by macroscopic systems (gas and liquid) and Theory of Fluctuations:** Considering a system is homogenous, it then can be divided into many identical subregions which are optically identical and act as scattering points smaller than the wavelength of the light. The light scattered by every subregions will interfere.

It is obvious that each subregion can always be paired with the others whose scattered electric fields are identical in amplitude but opposite in phase and will eventually cancel each other. In summary, no scattered light is observed in all direction except the zero angle.

In reality, no system are perfectly homogeneous. The properties of individual subregions fluctuate from the average properties. Therefore, the light scattered by each subregions does not have the same amplitudes and hence, it will not totally canceled by interference. Considering every subregion has a dielectric constant $\varepsilon$ embedded in a homogeneous medium with dielectric constant $\varepsilon_o$ and adopting the idea of interference in the previous section, we can obtain the Rayleigh ratio per unit volume in terms of the mean of the square of the fluctuation of dielectric constant $\overline{(\delta\varepsilon)^2}$ or $\overline{(\varepsilon-\varepsilon_o)^2}$

$$R_{VV} = \frac{\pi^2 V\overline{(\delta\varepsilon)^2}}{\lambda_o^4} \qquad \text{(A.1.11)}$$

where V is the volume of a subregion. Now we attempt to calculate the average fluctuation $\overline{(\delta\varepsilon)^2}$ in a subregion of size V. According to the theory of fluctuations, the system is allowed to spontaneously increase its Helmholtz free energy A and the time average fluctuation of Helmholtz free energy $\overline{\delta A}$ is expressed by

$$\overline{\delta A} = \frac{kT}{2} \qquad \text{(A.1.12)}$$

The fluctuation is measured from the lowest value of A, therefore the time-average value is always positive. Other independent variables (denoted by b) can fluctuate as well to the extent of producing $\overline{\delta A}$. The relationship between $\overline{(\delta b)^2}$ and A is given by

$$\overline{(\delta b)^2} = \frac{kT}{(d^2A/db^2)_{b=b_o}} \qquad (A.1.13)$$

where free energy A is a function of any independent variable of interest b and is always at a minimum as the property of interest b is equal to $b_o$.

**A.1.3.1 Scattering by gases and liquids:** When dealing with one-component gases and liquids, it is common to choose density ρ and temperature T as independent variables. For multicomponent systems such as polymer solution, polymer concentration have to be considered. Using eqs. (A.1.13) and thermodynamic relationships, fluctuation of density is easily obtained as

$$\overline{(\delta\rho)^2} = \frac{kT\rho^2\beta}{V} \qquad (A.1.14)$$

where V is again the volume of the subregion and β is its isothermal compressibility. Using the relationship between $\overline{(\delta\varepsilon)^2}$ and $\overline{(\delta\rho)^2}$,

$$\overline{(\delta\varepsilon)^2} = \left(\frac{d\varepsilon}{d\rho}\right)^2 \overline{(\delta\rho)^2} \qquad (A.1.15)$$

eqs. (A.1.11) and (A.1.14), we can obtain an general expression of Rayleigh ratio for gases and liquids in which only *density fluctuation* is considered

$$R_{VV} = \frac{kT\beta\rho^2\pi^2}{\lambda_o^4}\left(\frac{d\varepsilon}{d\rho}\right)^2 \qquad (A.1.16)$$

If we transform ε into $n^2$ by $\varepsilon = n^2$, we get

$$R_{VV} = \frac{4kT\beta n^2\rho^2\pi^2}{\lambda_o^4}\left(\frac{dn}{d\rho}\right)^2 \qquad (A.1.17)$$

It is believed that the dielectric constant does not change with temperature at constant density. Therefore the fluctuation of temperature does not cause fluctuation of the dielectric constant and does not raise scattering.

**Scattering by gases:** For dilute ideal gases, dielectric constant is

$$\varepsilon = 1 + 4\pi\alpha N \tag{A.1.18}$$

and the density of a gas is

$$\rho = \frac{MN}{N_A} \tag{A.1.19}$$

By applying eqs. (A.1.18), (A.1.19) and the definition of $\beta$ ( = 1/NkT) for an ideal gas into eqn. (A.1.16) gives

$$R_{VV} = \frac{N16\pi^4\alpha^2}{\lambda_o^4} \tag{A.1.20}$$

It is noted that the scattered intensity of an ideal gas is equal to the sum of the intensities scattered by individual molecules. This sample summation is only achieved in the condition of all individual scattering subregions being totally independent of each other.

**Scattering by liquids:** Molecules of liquids are not independent of each other. Total scattered light intensity is less than the sum of light scattered by individual molecules. The Rayleigh ratio is given by eqn. (A.1.16) or (A.1.17). Another source of fluctuation exists in liquids is the molecular orientation. This molecular orientation fluctuation leads to depolarized anisotropic scattering in which the direction of polarization of scattered field is not exactly vertically polarized when vertically polarized incident beam is used.

**A.1.4 Scattering by solutions of small molecules:** If we are only interested in the properties of solute molecules in the solution, we only consider the light scattered

from the source of the fluctuation of concentration of solute molecules in the solution. The fluctuation of dielectric constant which can related to the fluctuation of concentration is expressed by

$$\delta\varepsilon = \frac{d\varepsilon}{dn}\frac{dn}{dc}\delta c = 2n\frac{dn}{dc}\delta c \qquad \text{(A.1.21)}$$

The fluctuation of concentration is related to thermodynamic terms by eqn. (A.1.13)

$$\overline{(\delta c_2)^2} = \frac{kTM_2\phi_1}{(\partial\mu_2 / \partial c_2)_{P,T}} \qquad \text{(A.1.22)}$$

where $\mu$, chemical potential; $\phi$, volume fraction; c, concentration; M, molar mass. The subscript 2 refers to the solute molecules. Combining eqs. (A.1.21) and (A.1.22) into eqn. (A.1.11) gives the Rayleigh ratio arisen from the fluctuation of concentration

$$R_{VV} = \frac{4\pi^2 n^2 M_2\phi_1}{\lambda_o^4}\left(\frac{dn}{dc}\right)^2 \frac{kT}{(\partial\mu_2 / \partial c_2)_{P,T}} \qquad \text{(A.1.23)}$$

or simply

$$R_{VV} = KM\phi_1 \frac{RT}{(\partial\mu / \partial c)_{P,T}} \qquad \text{(A.1.24)}$$

where $K = \frac{4\pi^2 n^2}{NA\lambda_o^4}\left(\frac{dn}{dc}\right)^2$. If the solution is dilute enough, we can assume that the light scattered from a solution is composed of anisotropic scattering and density scattering from the solvent, and scattering by the fluctuation of solute concentration c. Therefore, in the experiment, the measured $R_{vv,\,solution}$ have to be subtracted by $R_{vv,solvent}$ so that the difference consists only the part from the fluctuation of concentration. The difference is called excess Rayleigh ratio $\Delta R_{vv}$. After replacing the derivative of chemical potential by its virial expansion

$$\left.\frac{\partial\mu}{\partial c}\right)_{P,T} = RT\frac{\phi_1}{c}(1+2A_2MC+\ldots) \qquad (A.1.25)$$

we get after rearrangement,

$$\frac{Kc}{\Delta R_{VV}} = \frac{1}{M}+2A_2c \qquad (A.1.26)$$

$Kc/\Delta R_{vv}$ is plotted against c where $\Delta R_{vv}$ is measured in different concentrations in the experiment, then M and $A_2$ are calculated from the y-intercept and slope respectively.

**A.1.4.1 Scattering from polymer solution:** Polymers are normally large compared to the wavelength of the light used. The particle scattering factor mentioned in section (A.1.2) have to be introduced in eqn. (A.1.26). Here we get

$$\frac{Kc}{\Delta R_{VV}} = \frac{1}{MP(\theta)}+2A_2c \qquad (A.1.27)$$

or simply

$$\frac{Kc}{\Delta R_{VV}} = \frac{1}{M}\left(1+\frac{1}{3}q^2R_g^2\right)+2A_2c \qquad (A.1.28)$$

where $P(\theta)^{-1}=1/(1-q^2R_g^2/3)\approx 1+q^2R_g^2/3$ if $q^2R_g^2 << 1$. In polymer science, it is common to treat polymers as polydisperse species. Therefore, eqn. (A.1.28) should be modified to

$$\frac{Kc}{\Delta R_{VV}} = \frac{1}{M_w}\left(1+\frac{1}{3}q^2 < R_g^2 >_z\right)+2A_2c \qquad (A.1.29)$$

where $M_w$, $<R_g^2>_z^{1/2}$ (or simply $<R_g>$) and $A_2$ are weight-average molar mass, root mean square z-average radius of gyration and second virial coefficient respectively. Eqn. (A.1.29) has three variables, $Kc/\Delta R_{vv}$, $q^2$ and c, which can be plotted in a xy plane by the means of Zimm plot. By measuring $\Delta R_{vv}$ in a set of q and c, we can plot $Kc/\Delta R_{vv}$ versus $q^2+P_1c$ where $P_1$ is a adjustable constant which makes the plot more nice. From the plot, $M_w$ is just the intercept $[Kc/\Delta R_{vv}]_{c\to 0,\ q\to 0}$. $R_g$ and $A_2$ can be

obtained from the slope of the lines of the plots $[Kc/\Delta R_{vv}]_{c\to 0}$ versus $q^2$ and $[Kc/\Delta R_{vv}]_{q\to o}$ versus c respectively.

## A.2 Dynamic laser light scattering (Dynamic LLS) [1,2,4]

As mentioned in the beginning of this chapter, the scattered light is slightly higher or lower than the original incident light frequency depending on whether the scattering points move towards or away from the detector which is the same case as the Doppler effect, or in other words, the frequency of the scattered light is slightly broader than that of the incident light. It is very difficult to detect this extremely small frequency broadening (~$10^5$ - $10^7$ Hz in comparison with the incident light frequency ~$10^{15}$ Hz) in the frequency domain by optical system, but it can be effectively transformed from time domain by measuring an intensity-intensity time correlation function $G^{(2)}(t,q)$.

When the scattering molecule is undergoing Brownian motion, the position vector **r** is a function of time and a random variable and $E_s$ has a randomly modulated phase. The scattered light is broadened in frequency with an optical frequency distribution $S(\omega)$ as illustrated in Figure A.2.1(a). Since the particle motion contains no preferred direction, the spectrum contains a continuous distribution of frequencies centered around $\omega_o$. The correlation function of the electric field $G^{(1)}(t)$ is also a measure of the frequency distribution and contains information on the molecular motion.[5-8] It is the Fourier transform of the power spectrum $S(\omega)$

$$G^{(1)}(t) = \left\langle E_s^*(0)E_s(t)\right\rangle \qquad (A.2.1)$$

where $\langle\ \rangle$ denotes a time or ensemble average and t is the correlation time

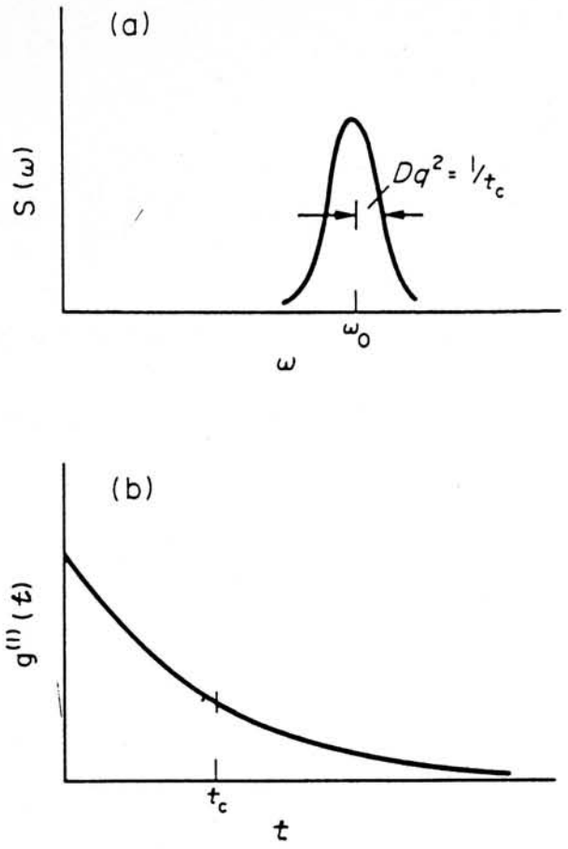


**Figure A.2.1** (a) Illustrate of an optical spectrum of scattered light; and (b) electric field correlation function

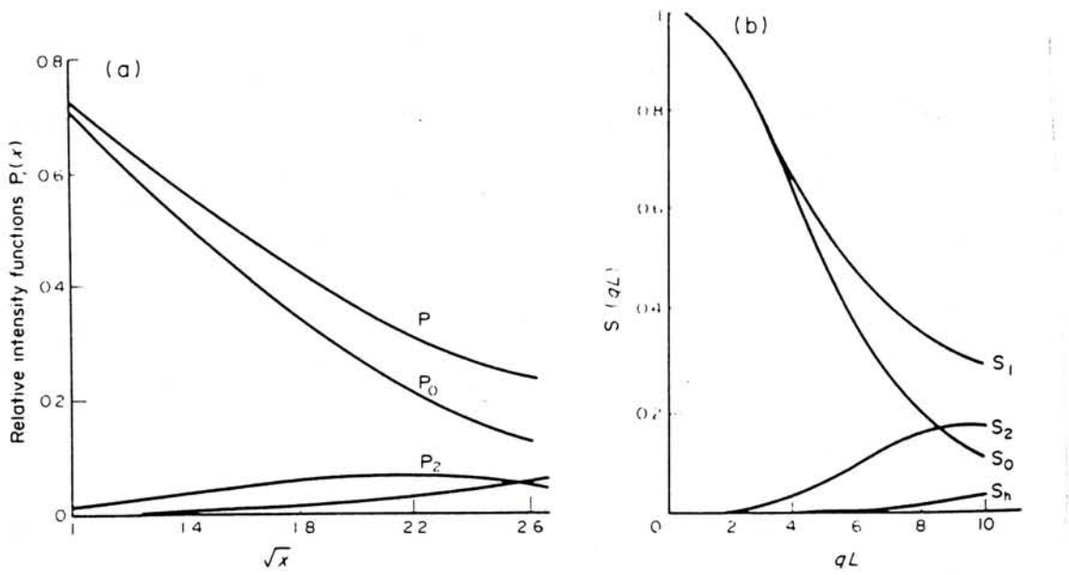


**Figure A.2.2** (a) Relative integrated intensities of light scattered from Gaussian coils versus $x^{1/2}$ ($qR_g$) (b) Relative integrated intensities of light scattered from rigid rod like polymers versus qL

$$S(\omega) = \frac{1}{2\pi}\int_0^\infty G^{(1)}(t)e^{-i\omega t}\,dt \qquad (A.2.2)$$

An illustration of a scattered optical spectrum and its normalized electric field time correlation function is shown in Figure A.2.1(b) The broadening of the Rayleigh-scattered light spectrum contains information on the motion of the scattering molecules.

The normalized electric field correlation illustrated in Figure A.2.1(b) is

$$g^{(1)}(t) = \frac{G^{(1)}(t)}{G^{(1)}(0)} \qquad (A.2.3)$$

In terms of amplitude and phase time dependence

$$g^{(1)}(t) = e^{-i\omega_o t}\,\frac{\langle A^*(0)A(t)\rangle}{\langle |A(0)|^2\rangle}\left\langle e^{-iq\cdot[r(t)-r(0)]}\right\rangle = e^{-i\omega_o t}C_A(t)C_\psi(t) \qquad (A.2.4)$$

where A(t) is the scattering amplitude per molecule and $C_A(t)$ and $C_\psi(t)$ are the amplitude and phase correlation functions. For small molecules (radius $R << q^{-1}$) or spherical molecules the amplitude part of the autocorrelation function becomes

$$C_A(t) = \frac{\langle A^*(0)A(t)\rangle}{\langle |A(0)|^2\rangle} = \qquad (A.2.5)$$

Then $g^{(1)}(t)$ carries information on the translational diffusion coefficient D through $C_\psi(t)$. This is related to the intermediate structure factor $G_s(r,t)$, which is the probability of finding a particle at position r at time *t* if it was at the origin at $t = 0$.

$$C_\psi(t) = \left\langle e^{-iq\cdot[r(t)-r(0)]}\right\rangle = \int G_s(\mathbf{r},t)e^{-iq\cdot r}d^3r \qquad (A.2.6)$$

where q [= $(4\pi n/\lambda_o)\sin(\theta/2)$] is defined before, the difference between the wave vectors of the scattered and incident waves, $n_1$ is the medium refractive index. For spherical identical scatters undergoing Brownian motion in solution

$$g^{(1)}(t) = e^{-Dq^2t}e^{-i\omega_o t} \tag{A.2.7}$$

The associated optical spectrum is

$$S(\omega) = \frac{\langle I_s \rangle Dq^2 / \pi}{(\omega - \omega_o)^2 + (Dq^2)^2} \tag{A.2.8}$$

which is a Lorentzian function centered at $\omega_o$ with a halfwidth $Dq^2$.

The translational diffusion coefficient D may be related to the molecular friction factor *f* through the Stokes-Einstein relation

$$D = \frac{kT}{f} \tag{A.2.9}$$

where k and T are the Boltzmann constant and the absolute temperature respectively. For a hard spherical with a radius of R, $f = 6\pi\eta R$, where $\eta$ is the viscosity of the solvent. For a polymer coil, R is replaced with its hydrodynamic radius $R_h$, so that

$$D = \frac{kT}{6\pi\eta \cdot R_h} \tag{A.2.10}$$

where k and T are the Boltzmann constant and the absolute temperature respectively.

When the molecular size is not much less than $q^{-1}$, the scattering intensity is reduced by intramolecular interference. For molecules with size ~ 1/q, the scattered intensity $I_s$ proportional to the particle scattering factor $P(\theta)$. For any shape of particle at small scattering angles, $P(\theta) = 1 - qR_g^2/3$ where $R_g$ is the radius of

gyration. If the molecule is not small and is not spherical or optically isotropic, then rotational diffusion will contribute a time dependent scattering amplitude; also for flexible molecules intramolecular dynamics gives a similar contribution.

The form of the correlation function $G^{(1)}$ can be calculated for model systems. For a rod-like molecule of length L, the dynamics of the molecule will contain contributions from translation and rotation. The form of $G^{(1)}(\tau)$ for a molecule having a rotational diffusion coefficient $\Theta$ is[9-11]

$$G^{(1)}(\tau) = I_s S(q,\tau) = I_s e^{-q^2 D\tau}\left[S_o + S_1 e^{-6\Theta\tau} + \ldots\right] \qquad \text{(A.2.11)}$$

where $S_o$, $S_1$ ... are weighting factors as shown in figure A.2.2 (b). For $qL \leq 3$, $S_o(qL)$ is dominant, while for $qL = 6$, $S_1 = 0.1$ and is significant compared with $S_o$.

For a flexible coil, the form of $G^{(1)}(\tau)$ is[12]

$$G^{(1)}(\tau) = I_s P(q,\tau) = I_s e^{-q^2 D\tau}\left[P_o + P_2 e^{-2\tau/\tau_1} + \ldots\right] \qquad \text{(A.2.12)}$$

where $P_o$, $P_2$ ... are weighting factors for the translational and internal modes of motion (figure A.2.2 (a)) and $\tau_1$ is first order internal relaxation time. For $qL \ll 1$, $P_o(qL)$ is dominant over $P_2$, $P_4$, ...

***A.2.1 Line-width measurement*:** The scattered light intensity is proportional to the square of the time average of the electric field

$$\text{Scattered intensity} = \langle I_s \rangle \propto \langle |E_s| \rangle^2 \qquad \text{(A.2.13)}$$

where $\langle\ \rangle$ denotes the time average. In order to measure the very small optical line-width generated from the frequency broadening of the optical spectrum, optical mixing techniques[13-15] are employed. There are two basic forms of optical mixing: heterodyne and homodyne (self-beat). By heterodyne mixing we refer to mixing the scattered light with a reference light wave (local oscillator) unshifted or shifted in

frequency from the incident light beam. In self-beat optical mixing the scattered wave is not mixed with a reference signal but is directly detected. Here we just consider the theory of self-beat detection. In self-beat detection the intensity autocorrelation function is determined as

$$G^{(2)}(t) = \lim_{T\to\infty} \frac{1}{2T} \int_{-T}^{T} I_s(0) I_s(t) dt \qquad \text{(A.2.14)}$$

It is the Fourier transform of the power spectrum and is readily measured by digital techniques. The normalized form of $G^{(2)}(t)$ is

$$g^{(2)}(t) = \frac{\langle E_s^*(0) E_s(0) E_s^*(t) E_s(t) \rangle}{\langle I_s \rangle^2} \qquad \text{(A.2.15)}$$

With some restrictions (such that the scattered field is a Gaussian random process), the correlation functions $g^{(1)}(t)$ and $g^{(2)}(t)$ are connected through the Siegert relation

$$g^{(2)}(t) = 1 + \left| g^{(1)}(t) \right|^2 \qquad \text{(A.2.16)}$$

Experimentally in self-beat dynamic light scattering the intensity autocorrelation function is measured as

$$g^{(2)}(t) = A\left[1 + \beta \left| g^{(1)}(t) \right|^2\right] \qquad \text{(A.2.17)}$$

Here A is a measured base line and $\beta$ is a geometric factor dependent on the coherence of detection.[16] The detector has an average photocurrent $\langle i \rangle$ which is proportional to the average light intensity $\langle i \rangle \propto \langle I_s \rangle$. Since the scattered light is normally at low level and in the form of discrete photon pulses, the scattered signal and hence correlation function is most usefully recorded using digital photon detection. In terms of photon counts

$$g^{(2)}(t) = \frac{1}{\langle n^2 \rangle} \sum_{i=1}^{N} n_i n_{i+p} \qquad \text{(A.2.18)}$$

where $t = p\Delta t$, $\Delta t$ = channel width, N = number of correlation channels and $\langle n \rangle$ = average number of photons counted in time $\Delta t$.

***A.2.2 Data analysis:*** In the case of polydisperse systems the general form of the time correlation function is the Laplace transform of a line-width distribution function $G(\Gamma)$

$$g^{(1)}(t) = \int_0^\infty G(\Gamma) e^{-\Gamma t} d\Gamma \qquad \text{(A.2.19)}$$

If the relaxation is diffusive, knowledge of $G(\Gamma)$ allows the molar mass on particle size distribution to be derived. The line-width $\Gamma$ usually depends on both C and $\theta$. This dependence can be expressed as[17-18]

$$\frac{\Gamma}{q^2} = D(1 + k_d C)(1 + f R_g^2 q^2) \qquad \text{(A.2.20)}$$

where D is the translational diffusion coefficient at C = 0 and q = 0, f is a dimensionless number, and $k_d$ is the diffusion second virial coefficient. The value of f depends on the chain structure, polydispersity, and solvent quality. Both thermodynamic and hydrodynamic interactions contribute to $k_d$, which can be further expressed as[19]

$$k_d = 2A_2 M_w - C_D N_A R_h^3 / M_w \qquad \text{(A.2.21)}$$

where $C_D$ is an empirical positive constant.

CONTIN, a general purpose and flexible computer program of inverting DLS data has been developed.[20] This has been widely applied in DLS studies with excellent results for DLS data having low noise. The program contains safeguarding

constraints to avoid the ill-posed nature of the inversion. An early method of analysis was based on a cumulant expansion[21,22] of the correlation function

$$\begin{aligned} \ln\left|g^{(1)}(t)\right| &= 1-\bar{\Gamma}t+\frac{1}{2!}\mu_2 t^2-\frac{1}{3!}\mu_3 t^3+\frac{1}{4!}\left[\mu_4-3\mu_2^2\right]t^4+\ldots.. \\ &= 1+\sum_{m=1}^{\infty}k_m(\Gamma)\frac{-t^m}{m!} \end{aligned} \qquad \text{(A.2.22)}$$

where $k_m=\left[(-1)^m\frac{d^m}{dt^m}\ln\left|g^{(1)}(t)\right|\right]_{t=0}$ is the $m^{th}$ cumulant of $g^{(1)}(t)$ and $\mu_i=\int_0^{\infty}(\Gamma-\bar{\Gamma})^i\,G(\Gamma)d\Gamma$. Equation (A.2.22) may be fitted by a least squares routine to the correlation function and values for $\mu_2$, $\mu_3$, ... obtained. The average width $\bar{\Gamma}=\int_0^{\infty}\Gamma G(\Gamma)\,d\Gamma$ is the mean relaxation time. The variance is $\mu_2/\bar{\Gamma}^2$, where $\mu_2=\int_0^{\infty}(\Gamma-\bar{\Gamma})^2\,G(\Gamma)\,d\Gamma$. For low q, qR < 1 and $\bar{\Gamma}=\bar{D}q^2$, where $\bar{D}$ is a z-average.

## A.7 References


1 Chu, B. *Laser Light Scattering*, 2nd Ed; Academic Press: New York, 1991.

2 Pecora, R.; Berne, B. *J. Dynamic Light Scattering;* Plenum Press: New York, 1976.

3 Munk, P. *Introduction to macromolecular science*; John Wiley & Sons, Inc.: Singapore, 1989

4 King, T. A. In *Comprehensive Polymer Science, vol. 1*; Booth, C.; Price, C., Eds.; Pergamon Press: Oxford, 1989; chap. 7.

5 Degiorgio, V.; Lastovka, J. B. *Phys. Rev. A* **1971**, *4*, 2033.

6 Cummins, H. Z.; Pike, E. R., Eds. *Photon Correlation and Light Beating Spectroscopy*; Plenum Press: New York, 1974.

7 Cummins, H. Z.; Pike, E. R., Eds. *Photon Correlation and Light Beating Spectroscopy*; Plenum Press: New York, 1977.

8 Ware, B. R. In *Optical Techniques in Biological Research*; Rousseau, D. L., Ed.; Academic Press: New York, 1984; p 1.

9 Pecora, R. *J. Chem. Phys.* **1965**, *43*, 1562.

10 Cummins, H. Z.; Carlson, F. D.; Herbert, T. J.; Woods, G. *Biophys. J.* **1969**, *9*, 518.

11 Bauer, D. R.; Brauman, J. I.; Pecora, R. *Macromolecules* **1975**, *8*, 443.

12 Pecora, R. *J. Chem. Phys.* **1968**, *49*, 1032.

13 Glauber, R. J., Ed. *Quantum Optics*; Academic Press: New York, 1969.

14 Kay, S. M.; Maitland, A., Eds. *Quantum Optics*; Academic Press: New York, 1970.

15 Loudon, R. *The Quantum Theory of Light*; Oxford University Press: Oxford, 1983.

16 Jakeman, E.; Oliver, C. J.; Pike, E. *J. Phys. A: Gen. Phys.* **1970**, *3*, L45.

17 Stockmayer, W. H.; Schmidt, M. *Pure & Appl. Chem.* **1982**, *54*, 407.

18 Stockmayer, W. H.; Schmidt, M. *Macromolecules* **1984**, *17,* 509.

19 Yamakawa, H. *Modern Theory of Polymer Solutions*; Harper and Row; New York, 1971.

20 Provencher, S. W. *Comp. Phys. Commun.* **1982**, *27*, 229.

21 Koppel, D. E. *J. Chem. Phys.* **1972**, *57*, 4814.

22 Lee, S. P.; Chu, B. *Appl. Phys. Lett.* **1974**, *24*, 575.